ORP2, a cholesterol transporter, regulates angiogenic signaling in endothelial cells

Koponen, Annika

2020-11

Koponen , A , Pan , G , Kivelä , A M , Ralko , A , Taskinen , J H , Arora , A , Kosonen , R , Kari , O K , Ndika , J , Ikonen , E , Cho , W , Yan , D & Olkkonen , V M 2020 , ' ORP2, a cholesterol transporter, regulates angiogenic signaling in endothelial cells ' , FASEB Journal , vol. 34 , no. 11 , pp. 14671-14694 . https://doi.org/10.1096/fj.202000202R

http://hdl.handle.net/10138/352495
https://doi.org/10.1096/fj.202000202R

acceptedVersion

ORP2, a cholesterol transporter, regulates angiogenic signaling in endothelial cells

Annika Koponen[1], Guoping Pan[2], Annukka M. Kivelä[1], Arthur Ralko[3], Juuso Taskinen[1], Amita Arora[1], Riikka Kosonen[1], Otto K. Kari[4], Joseph Ndika[5], Elina Ikonen[1,6], Wonhwa Cho[3], Daoguang Yan[2] and Vesa M. Olkkonen[1,6*]

[1]*Minerva Foundation Institute for Medical Research, Biomedicum 2U, FI-00290 Helsinki, Finland*

[2]*Department of Biology, Jinan University, 510632 Guangzhou, China*

[3]*Department of Chemistry, University of Illinois at Chicago, Chicago, Illinois 60607-7061, USA*

[4]*Drug Research Program, Division of Pharmaceutical Biosciences, Faculty of Pharmacy, FI-00014 University of Helsinki, Finland*

[5]*Human Microbiome Research, Faculty of Medicine, University of Helsinki, P.O. Box 21, FI-00290 Helsinki, Finland*

[6]*Department of Anatomy, Faculty of Medicine, FI-00014 University of Helsinki, Finland*

Key words: angiogenesis, cholesterol trafficking, Osbpl2, VEGF receptor

Short title: Function of ORP2 in angiogenesis

*Address correspondence to Vesa Olkkonen, Minerva Foundation Institute for Medical Research, Biomedicum 2U, Tukholmankatu 8, FI-00290 Helsinki, Finland
Tel. +358-50-4112297; E-mail: vesa.olkkonen@helsinki.fi

Abbreviations

EC	Endothelial cell
HUVEC	Human umbilical vein endothelial cell
KD	Knock-down
MβCD	Methyl-β-cyclodextrin
MMP	Matrix metalloproteinase
ORP	OSBP-related protein
OSBP	Oxysterol-binding protein
$PI(4,5)P_2$	Phosphatidylinositol-4,5-bisphosphate
PIP	Phosphatidylinositol phosphate
PM	Plasma membrane
VEGF	Vascular endothelial growth factor
VEGFR	VEGF receptor

Abstract

Oxysterol-binding protein related protein 2 (ORP2), a cholesterol–PI(4,5)P_2 countercurrent transporter, was recently identified as a novel regulator of plasma membrane (PM) cholesterol and PI(4,5)P_2 content in HeLa cells. Here, we investigated the role of ORP2 in endothelial cell (EC) cholesterol and PI(4,5)P_2 distribution, angiogenic signaling and angiogenesis. We show that ORP2 knock-down modifies the distribution of cholesterol accessible to a D4H probe, between late endosomes and the PM. Depletion of ORP2 from ECs inhibits their angiogenic tube formation capacity, alters the gene expression of angiogenic signaling pathways such as VEGFR2, Akt, mTOR, eNOS and Notch, and reduces EC migration, proliferation and cell viability. We show that ORP2 regulates the integrity of VEGFR2 at the PM in a cholesterol-dependent manner, the depletion of ORP2 resulting in proteolytic cleavage by matrix metalloproteinases and reduced activity of VEGFR2 and its downstream signaling. We demonstrate that ORP2 depletion increases PM PI(4,5)P_2 coincident with altered F-actin morphology, and reduces both VEGFR2 and cholesterol in buoyant raft membranes. Moreover, ORP2 knock-down suppresses expression of the lipid raft-associated proteins VE-cadherin and caveolin-1. Analysis of the retinal microvasculature in ORP2 knock-out mice generated during this study demonstrates subtle alterations of morphology characterized by reduced vessel length and increased density of tip cells and perpendicular sprouts. Gene expression changes in the retina suggest disturbance of sterol homeostasis, down-regulation of VE-cadherin, and a putative disturbance of Notch signaling. Our data identifies ORP2 as a novel regulator of EC cholesterol and PI(4,5)P_2 homeostasis and cholesterol-dependent angiogenic signaling.

INTRODUCTION

Cholesterol is considered an indispensable component of cellular membranes. Not only does it serve as a structural component and regulator of membrane biophysical properties, but it is also a major component of plasma membrane (PM) lipid rafts where it functions as a platform for multiple signaling processes (1, 2). In endothelial

cells (ECs) cholesterol and its efficient transport have a particularly important role, given the function of these cells as a barrier between the circulation and the tissues, their abundant vectorial transport tasks, and their richness in lipid rafts including caveolae. Accordingly, disturbances in EC lipid order are suggested to be causative factors in diseases such as atherosclerosis, type 2 diabetes and cancers. Recently, PM cholesterol has proven to play an important role in the regulation of angiogenesis, i.e. in the formation of new blood vessels from pre-existing ones (3-6). However, the factors and detailed mechanisms linking cholesterol transport to angiogenesis remain poorly understood.

Vascular endothelial growth factor (VEGF) is a major initiator of angiogenic signaling and vessel formation in ECs. VEGF binds to the extracellular domain of its major receptor, vascular endothelial growth factor receptor 2 (VEGFR2), inducing receptor dimerization and autophosphorylation of its intracellular tyrosine residues leading to the activation of downstream effectors such as PI3K/Akt, ERK, FAK and eNOS (7). The activation of these signaling pathways results in increased cell viability, proliferation and migration as well as increased barrier permeability, functions essential for the initiation of angiogenesis. Several recent reports suggest that PM cholesterol and the integrity of lipid rafts are crucial for VEGFR2 signaling, and that perturbations of intracellular cholesterol transport result in impaired angiogenesis (3, 5, 6, 8).

Oxysterol-binding protein homologs, ORPs, constitute a ubiquitously expressed family of lipid-binding proteins with various functions in lipid transport and signaling. ORPs are typically localized at membrane contact sites (MCSs), where they generate and maintain organelle-specific lipid compositions (9). ORP2 encoded by *OSBPL2* has a lipid-binding cavity with affinity for oxysterols, cholesterol and phosphatidylinositol phosphates (PIPs). ORP2 has several documented cellular functions related to cholesterol homeostasis, triglyceride metabolism, cell adhesion, migration, proliferation (10-14) and steroid hormone synthesis in adrenocortical cells (15). ORP2 targets lipid droplet-endoplasmic reticulum MCSs, late endosomes (LE) and the plasma membrane (PM) where it co-localizes with lamellipodial F-actin and induces PM protrusions. Recently ORP2 was proposed by us and others (16, 17) to regulate the intracellular transport of cholesterol to the PM by transferring cholesterol in exchange for $PI(4,5)P_2$ and thus controlling the PM lipid composition.

In the present work we assess the role of ORP2 in EC cholesterol trafficking and angiogenesis *in vitro* and *in vivo*. We show that the knock-down (KD) of ORP2 accumulates D4H-accessible cholesterol in LEs reducing its distribution to the PM, reduces cholesterol in a buoyant raft fraction, and causes disturbances in angiogenic signaling. We identify ORP2 as a novel regulator of VEGFR2 signaling and show that ORP2 KD causes VEGFR2 cleavage at the PM of ECs and inhibits the activity of the receptor and its downstream targets upon VEGF stimulus. ORP2 KO mice present with a subtle alteration of retinal angiogenesis, supporting the relevance of the observations *in vivo*.

MATERIALS AND METHODS

Antibodies and reagents

The primary antibodies used are specified in Supplementary Table S1. The secondary fAlexa Fluor-488 anti-mouse IgG was from Molecular Probes/Invitrogen (Carlsbad, CA), Cy5® anti-rabbit from Life Technologies (Eugene, OR) and Oregon Green® 488 Phalloidin from Thermo Scientific (Waltham, MA).

The Strep-Tactin® XT magnetic beads were purchased from IBA Lifesciences (Goettingen, DE), NeutrAvidin agarose beads from Thermo Scientific, and Protein G Magnetic beads from Pierce/Thermo Scientific. The Sulfo-NHS-SS-Biotin for cell surface receptor biotinylation was purchased from Thermo Scientific and the matrix metalloproteinase (MMP) inhibitor Marimastat from Sigma-Aldrich (Saint Louis, MO). The Silencer Select® OSBPL2 and the Negative Control #2 siRNA were from Ambion/Thermo Scientific (Austin, TX). Puromycin was purchased from Gibco/Fisher Scientific (Loughborough, UK), *in vitro* Angiogenesis assay kit (ECM625) from Millipore (Burlington, MA) andVEGF-A_{165} from R&D Systems (Minneapolis, MN).

cDNA constructs

Human ORP2 wild-type, phosphoinositide-binding deficient (mHHK; $H^{178\text{-}179}A$, $K^{423}A$), sterol-binding deficient (ΔELSK; deletion of E87-K90) mutants in pmCherry-C1 (Clontech/Takara Bio) were described in (18), and GFP-tagged versions of these mutants were generated by transferring the cDNAs into BglII/KpnI restriction sites of

the pEGFP-C1 vector (Clontech/Takara Bio). The mCherry-D4H cholesterol probe plasmid was a kind gift from Prof. Gregory Fairn (Department of Biochemistry, University of Toronto, ON).

Generation of ORP2 shRNA expressing lentiviruses

The generation of a lentiviral ORP2-2xStrep expression construct is described in (16). The ORP2 knock-down lentiviruses were generated by using shRNA clones TRCN000154381 and TRCN0000429830 in pLKO.1 (Sigma-Aldrich). The non-target shRNA control lentivirus was generated from SHC002 (Sigma-Aldrich) and the overexpression control lentivirus from an empty pENTR2b vector recombined with pLenti6.3/V5-DEST (Invitrogen). The lentiviruses were packaged by the Biomedicum Functional Genomics Unit (the HiLIFE Institute, Helsinki, Finland).

Addressing possible shRNA off-target effects

The possible off-target effects of ORP2 shRNA were addressed by conducting all of the ORP2 gene silencing experiments (excluding the next generation RNA sequencing) with two independent shRNAs: TRCN000154381 and TRCN000429830. The next generation RNA sequencing was performed on HUVEC shORP2 samples silenced with TRCN000154381, and the putative off-target genes of the RNA sequencing results, i.e. the genes where a seed sequence identical to the used shRNA was found, were excluded from the data before further analysis by using the GESS algorithm (19).

Cell culture and genetic manipulations

Human umbilical vein endothelial cells (HUVECs), the EC growth medium Endothelial Cell Growth Medium v2 (ECGM2) and the ECGM2 Supplement Mix were purchased from PromoCell (Heidelberg, DE). The cells were grown in Fibronectin 10 µg/ml - gelatin 0.05% (Sigma-Aldrich) coated flasks/plates in a 37°C humidified incubator. For cDNA transfections by electroporation, the Nucleofector™ Kit (Lonza, Basel, CH) for HUVECs was used according to Amaxa™ Optimized Protocol. For lentivirus-mediated transductions, HUVECs were incubated for 48 h with either fresh or concentrated lentiviruses using a multiplicity of infection (MOI)

of 10, followed by 24-h antibiotic selection with 2.5 μg/ml puromycin for lentivirus-mediated shRNA silencing.

Fluorescence microscopy

The fluorescent labels were visualized with a Zeiss Axio Observer Z1 microscope equipped with PInApo x63/1.40 oil DICII objective and a Colibri LED light source (Zeiss, Oberkochen, DE). Images were taken with an AxioCam HRm camera and recorded with Zen 2 v.2.0.0 software (Zeiss). Adobe Photoshop CC 2017 (Adobe, San Jose, CA) and Image J/Fiji (National Institutes of Health, Bethesda, MD) were used for image processing and analysis.

Preparation of PI(4,5)P_2 sensor

The PI(4,5)P_2 sensor was prepared from the engineered epsin 1 ENTH domain as described previously (20). Briefly, the engineered epsin 1 ENTH domain was expressed as a glutathione-S-transferase (GST)-tagged protein in *E. coli* BL21 RIL codon plus (Stratagene, San Diego, CA) cells and purified using the GST–affinity resin (GenScript, Piscataway, NJ). The purified protein was labeled at a single Cys with acrylodan to generate a ratiometric sensor. The sensor was calibrated using giant unilamellar vesicles with the lipid composition stipulating that of the inner leaflet of the plasma membranes of mammalian cells (20-22).

Measurement of plasma membrane PI(4,5)P_2 content

HUVECs were seeded (5 x 10^4 cells) into 50-mm round glass–bottom plates (MatTek, Ashland, MA) and grown in 2 ml of ECGM2 (PromoCell) supplemented with ECGM2 Supplement Mix (PromoCell) at 37^{o}C in a humidified atmosphere with 5% CO_2. Cells were transfected with the freshly packaged lentivirus encoding ORP2 or control shRNA (100 μl) using 1.1 μl of polybrene (10 μg/ml) and allowed to grow for 48 hours, followed by treatment with puromycin (2.5 μg/ml) for 24 hours. The PI(4,5)P_2 sensor was delivered into the cells by microinjection and PI(4,5)P_2 in the inner leaflets of the plasma membrane (PM) was quantified using a custom-modified Olympus FV3000 confocal microscope as described previously (20). All data acquisition and ratiometric imaging data analyses were performed as described in (20-22). The PI(4,5)P_2 concentration at the PM of a single HUVEC cell was determined in

a spatiotemporally resolved manner and spatially averaged at a given time. Each data set was collected from a minimum of 15 different cells and averaged.

The $PI(4,5)P_2$ content was also measured from the PM of ORP2 KD and control HUVECs by utilizing a competitive $PI(4,5)P_2$ ELISA Kit (Echelon Biosciences, Salt Lake City, UT). Approximately 20 x 10^6 HUVECs transduced by either shORP2 or shCTRL virus were collected and the PM of the cells was isolated by Minute™ Plasma Membrane Kit (Invent Biotechnologies, Plymouth, MN) according to manufacturer's protocol. The lipids of the obtained PM pellet were extracted according to the instructions of the $PI(4,5)P_2$ ELISA Kit, and the $PI(4,5)P_2$ content of the PM lipids was determined with an EnSpire fluorometer/multimode plate reader (Perkin Elmer, Waltham, MA). The results were normalized to the cytosolic protein content of the respective cell samples (BCA assay, Pierce/Thermo Fisher Scientific).

Measurement of plasma membrane cholesterol content

For the PM cholesterol content measurements, the PM of ORP2 KD and control HUVECs was isolated by Minute™ Plasma Membrane Kit (Invent Biotechnologies, Plymouth, MN) as described above, and the PM cholesterol concentration was determined by using the Amplex Red assay (Thermo Fisher Scientific) according to the manufacturer's instructions. The results were normalized by the protein content of the PM samples (BCA assay, Pierce/Thermo Fisher Scientific).

For assaying the cholesterol pool of the extracellular leaflet of the PM, purified His_6-ALOD4 obtained as a gift from Prof. Arun Radhakrishnan (Univ. of Texas Southwestern Medical Center, Dallas) was used as described in (23). Briefly, the cells were incubated with growing concentrations (0 µM, 3 µM and 10 µM) of His_6-ALOD4 for 1 hour at 37°C, rinsed with PBS and lysed. The association of the probe with cell surface cholesterol was analyzed from the lysates by western blot with anti-His_6 antibody (ABclonal, Woburn, MA).

EC in vitro angiogenesis assay

In vitro angiogenesis assay (Millipore) was performed according to the manufacturer´s protocol. After 48-h lentivirus transduction, $1.5x10^4$ cells were seeded on ECM Matrix™ and incubated at +37°C for 12 h. Tube formation was visualized under an inverted light microscope with 4x magnification and the images were

acquired with Evos XL Cell Imaging System (AMG; Thermo Fisher Scientific). Images were analyzed by using Angiogenesis Analyzer of ImageJ.

RNA sequencing and analysis of differential gene expression

For RNA sequencing sample preparation, HUVECs were transduced with shORP2 or control lentivirus for 48 h, followed by 24-h antibiotic selection with 2.5 µg/ml of Puromycin (Gibco). The RNA was isolated from cell lysates with the Qiagen RNeasy^{TM} Mini kit (Hilden, DE) according to the manufacturer's protocol. Genomic DNA background was depleted prior to sequencing by DNAse treatment (Qiagen).

Differential expression analysis was performed using the Chipster suite (24), and the following workflow was used to generate the differential expression data: Single-end reads were aligned to the reference genome GRCh38, with Bowtie2 (25). Mapped reads were counted using HTseq with the ENSEMBL GRCh38 annotation file as a reference (26). Finally, differential expression analysis was performed using DESeq2, with a cut-off value for Benjamini-Hochberg adjusted p-values of 0.05 (27). Over-representation analysis of significantly differentially expressed genes was performed using the ConsensusPathDB web application (28), available at: http://ConsensusPathDBdb.org. Wikipathways, KEGG, Reactome and PID were selected as the most relevant databases for the pathway analysis of this study.

Strep-Tactin pull down and ORP2 interactome analysis

HUVECs were grown on 10 cm dishes and transduced with ORP2-2xStrep or overexpression control lentivirus for 48 h. Subsequently, the cells were lysed in freshly prepared lysis buffer [10 mM HEPES (pH 7.6), 150 mM NaCl, 0.5 mM $MgCl_2$, 10% glycerol, 0.5% Triton X-100, Protease inhibitor cocktail], and cell debris was removed by centrifugation at 20 000 x g for 15 min. The lysates were first incubated with Protein G Magnetic Beads (Pierce/Thermo Scientific) for 30 min at 4°C to remove unspecifically bound material, and then with Strep-Tactin® XT Magnetic Beads (IBA Lifesciences) o/n. After washing the beads twice with lysis buffer and 10 mM HEPES (pH 7.6), 150 mM NaCl, the samples were solubilized in 0.2% RapiGest SF (Waters Inc., Milford, MA). The protein concentration was determined with the BCA protein assay (Thermo Fisher Scientific, Waltham, MA, USA) and the samples were adjusted to a final protein amount of 10 µg in 50 µl in

AMBIC (Thermo Fisher Scientific). On-beads digestion was conducted with the In-solution tryptic digestion and guanidination kit (Thermo Fisher Scientific) without guanidination. After digesting the samples overnight, formic acid was added ad 0.1%, followed by a 45-min incubation at 37 °C and 15-min centrifugation at 13,000 rpm. Tryptic peptides were further cleaned using Pierce C18 spin columns (Thermo Fisher Scientific). Eluted peptides were dried in a speed vac, and resuspended in 0.1% formic acid. Samples were loaded into an Easy-nLC 1200 (Thermo Fisher Scientific) in 250 µl autosampler microvials. Chromatographic separation of 100 ng of peptides was carried out in commercially packed Acclaim PepMap C18 columns (2 mm, 100 Å, 75 mm, 15 cm) (Thermo Fisher Scientific). Peptides were loaded in buffer A (5% acetonitrile and 0.1% formic acid) and eluted with a 1-hour linear gradient from 5% to 30% buffer B (80% acetonitrile and 0.1% formic acid). Each sample was run three times, with 15-min wash runs between every injection. Mass spectra were acquired using a Top N data-dependent method with an automatic switch between full MS and MS/MS (MS2) scans with an Orbitrap Fusion instrument (Thermo Fisher Scientific). The acquisition parameters for the full MS scan were 120,000 resolution, 350 to 1800 m/z mass range, and a 4e5 ions AGC target, followed by a 30,000 resolution and 5e4 ions AGC target, with a 2 m/z isolation window and a 30 s dynamic exclusion for MS2 spectra acquisition. Protein groups identification and quantification were carried out with MaxQuant v. 1.6.1.0 (29) using the UniProtKB FASTA file for human containing 86725 entries, to which 245 common contaminants and all reverse sequences were added. Data was extracted and filtered for further analysis using the Perseus data analysis software v. 1.6.5.0 (30). Histone and ribosomal peptide IDs were removed as putative contaminants, and only peptide IDs with >5-fold enrichment in the ORP2-2xStrep sample compared to control sample were included in the final data set.

Cell morphology assessment

The morphology of the shORP2 HUVECs as compared to the controls was assessed visually under a bright-field microscope and images were acquired with an Evos XL Cell Imaging System (AMG; Thermo Fisher Scientific). Changes in actin cytoskeleton morphology were visualized by Oregon green phalloidin dye and in focal adhesions by anti-phospho-paxillin(Tyr118) antibody with a Zeiss Axio

Observer Z1 fluorescent microscope. The cell spreading/perimeter analysis was conducted with ImageJ particle analysis function for >200 cells (n=3).

EC migration assays

Endothelial cell migration was assessed both under planar unstimulated conditions and as growth factor-stimulated directional trans-filter movement in real-time.

The planar migration was monitored using IncuCyte ZOOM Scratch Wound assay (Essen BioScience, Hertfordshire, UK). $3x10^4$ HUVECs were seeded in a 96-well Image Lock plate along with control or ORP2 shRNA lentivirus in complete ECGM2 media. Cells were incubated for 48 h at 37°C in a humidified atmosphere with 5% CO_2, followed by antibiotic selection using 2.5 µg/ml puromycin for 24 h. For wound healing assay, a uniform scratch wound was made in each well using IncuCyte Wound maker. Wells were then rinsed with PBS to remove floating cells and fresh ECGM2 complete media was added. Cell migration was imaged using IncuCyte Zoom microscope for 24 h with 2-h intervals using a 4x objective. Relative wound density was used to quantify wound closure using IncuCyte Cell migration software.

The trans-filter migration of control or ORP2 shRNA transduced HUVECs was measured with xCELLigence™ Real-Time Cell Analysis system equipped with a DP instrument (ACEA Biosciences, San Diego, CA). After 48-h lentiviral transduction and puromycin selection (as described earlier), the cells were starved for 2 h (ECGM2 without supplements) and then seeded at a density of $3x10^4$ cells/well into upper chamber of xCELLigence CIM-plate™ 16 (ACEA Biosciences) containing starvation media. The wells of the lower chamber were loaded with ECGM2 media with double supplements and 50 ng/ml VEGF-A (R&D Systems). The stimulated directional trans-filter cell migration from the upper to the lower chamber was detected by electrical impedance for 24 h at 10-minute intervals. The measurements were performed at 37°C, in a humidified 5% CO_2 atmosphere and recorded with Real-Time Cell Analysis (RTCA) Software 1.2 (ACEA Biosciences).

EC viability and proliferation measurements

To determine the effects of ORP2 KD on cell survival, we performed a viability assay based on the enzymatic reduction of the tetrazolium salt MTT (Thermo Scientific) by metabolically active cells. HUVECs were seeded in 96-well microtiter plates in

ECGM2 medium and allowed to attach for 24 h. After confluency was reached, the cells were starved for 2 h and treated with 50 ng/ml of VEGF (R&D Systems) for 12 h. The cell viability was determined by incubating the cells for 4 h at 37°C with 5 mg/ml MTT, following removal of medium and cell solubilization into 100 µl of DMSO. The colorimetric change of MTT was measured at 570 nm with EnSpire fluorometer/multimode plate reader (Perkin Elmer). The results are shown as mean ± SD of 4 independent experiments, each with 5 replicate wells. The real-time proliferation efficiency of ORP2 KD HUVECs was determined by xCELLigence® instrument as described in (10).

Cell fractionation for lipid raft isolation

For detergent-free lipid raft isolation, shORP2 and shCTRL lenti-transduced HUVECs (approximately $2x10^6$ cells/sample) were collected by scraping into PBS, pelleted by centrifugation at 200 x g for 5 min and resuspended into 0.5 M sodium carbonate buffer (pH 11.0) containing protease inhibitor cocktail (Roche, Basel, Switzerland). The cells were homogenized by forcing them 150 x through a 23-gauge needle. Subsequently, the samples were adjusted to 45% sucrose by addition of 90% sucrose and transferred into ultracentrifuge tubes. A 5% to 35% discontinuous sucrose gradient was generated on top of the samples (6), and ultracentrifugation was carried out at 190,000 x g for 22 h in a TLS-55 swinging bucket rotor (Beckman, Brea, CA). After the centrifugation, nine fractions were collected from the top. The light membrane fraction, i.e. the lipid raft fraction (fraction 4), as well as fractions 5 & 6 were selected for further analysis. The distribution of VEGFR2, Flotillin-1 and β-tubulin between the membrane and the soluble fractions were analyzed by western blot with the respective antibodies. Cholesterol content of the gradient fractions was measured by using the Amplex Red assay (Thermo Fisher Scientific) and normalized by the protein content of the fractions (BCA assay, Pierce/Thermo Fisher Scientific).

VEGF receptor biotinylation assay

To isolate the surface pool of VEGFR2 in HUVECs, the cell surface proteins of shORP2 or shCTRL lenti-transduced cells were biotinylated with the membrane impermeable Sulfo-NHS-SS-biotin reagent (Thermo Scientific) according to the

manufacturer's protocol. After biotinylation the cells were washed three times with quenching buffer (50 mM Tris, pH 8.0) and lysed into 10 mM HEPES (pH 7.6), 150 mM NaCl, 0.5 mM $MgCl_2$, 10% glycerol, 0.5% Triton X-100, 0.5% sodium deoxycholate containing protease inhibitor cocktail. The cell debris was removed by centrifugation at 14 000 x g for 10 min at 4°C, after which a sample was taken from the supernatant representing the total pool of VEGFR2. The rest of the lysate was mixed with NeutrAvidin agarose beads (Thermo Scientific) and incubated in rotation for 4 h. The beads were collected and washed twice with lysis buffer, and the bead-bound cell surface receptors extracted for western blot by boiling with SDS-PAGE sample buffer. The remaining lysate represented the intracellular VEGFR2 pool.

Plasma membrane cholesterol depletion & loading

The PM cholesterol of HUVECs was depleted by 30-60-min incubations with 4.6 mM methyl-β-cyclodextrin (MβCD) at 37°C. PM cholesterol rescue of the *in vitro* angiogenic tube formation assay was performed by 3-hour incubation with 4 mM MβCD-cholesterol at 37°C. Both the MβCD and the MβCD-cholesterol complex were purchased from Sigma-Aldrich.

Generation of ORP2 knock-out (KO) mice by CRISPR/Cas9

Osbpl2(ORP2) KO mice were generated by Shanghai Biomodel Organism Science and Technology Development Co., Ltd. by CRISPR/Cas9. Exon 3 of Osbpl2 was removed by targeting its flanking intronic regions with four gRNAs (Supplementary Fig. S1A-D). The gRNAs and Cas9 mRNA were produced by *in vitro* transcription and microinjected into fertilized C57BL/6J eggs. From the F0 mice, the Osbpl2 gene region was PCR amplified and sequenced via a T-vector. Founders with deletions removing exon 3 were selected for further breeding. In these animals, Osbpl2 protein translation is halted by a premature termination codon, resulting in a truncated protein of 31 amino acid residues: MNGEEEFFDAVTGQPFLLPCSPEATSVCGVS. In this study we only investigated the retinal vasculature of the KO animals, relevant for the present topic. The animal experiments were approved by the Ethics Committee for Animal Experiments of Jinan University and performed in compliance with the China government guidelines. Mice were housed in sterilized filter-top cages and given unlimited access to food and water with 12/12-h dark/light cycle.

Retinal vasculature analysis of ORP2 KO mice

Eyes from humanely terminated postnatal day 7 (P7) mouse pups were enucleated into cold PBS and fixed in 4% paraformaldehyde (PFA) at 4°C for 2 h. Then the eyes were transferred into cold PBS on ice for 5 - 10 min. Retinas were dissected, created into a 'petal' shape, and fixed in MeOH at −20°C. After brief washes in cold PBS, retinas were incubated in 100 µl of Perm/Block solution (PBS, 0.3% Triton, 0.2% BSA) + 5% fetal calf serum and shaken gently for 1 h. After removing the Perm/Block solution the retinas were incubated with gentle shaking overnight at 4 °C with 100 µl FITC-conjugated Isolectin B4 (Sigma-Aldrich, 40 µg/mL in Perm/Block). After four washes in PBS, 0.3% Triton X-100, retinas were transferred onto microscope slides and imaged with a confocal microscope (Olympus FV3000). All images were photo-merged with Toupview and analyzed with Image Pro Plus 6.0.

Gene expression analysis in mouse endothelia

Total RNA was isolated from P7 mouse pups retina with TRIzol reagent (Invitrogen/Thermo Scientific) according to the manufacturer's instructions. RNA samples were reverse transcribed by the PrimeScript™ RT reagent Kit with gDNA Eraser (Takara Bio, Kusatsu, JP). qRT-PCR was performed with TB Green™ Premix Ex Taq™ (Takara Bio) using a instrument CFX 96 (Bio-Rad) and analyzed by CFX ManagerTM software using $-\Delta\Delta C_T$ method, with actin as an endogenous reference. Relative expression is represented as the ratio of target gene to reference from littermate pups. The primer sequences used are shown in Supplementary Fig. S1E.

RESULTS

ORP2 controls the distribution of cholesterol in HUVECs

We and others recently proposed that ORP2 is involved in the intracellular delivery of cholesterol to the PM in HeLa cells (16, 17). As efficient cholesterol transport is particularly important for the maintenance of healthy endothelia, we investigated the effects of ORP2 on cholesterol distribution in primary endothelial cells, HUVECs. The cells were transfected with the cholesterol-binding domain 4 of *C. perfringens* theta-toxin fused with mCherry (mCherry-D4H) and with either ORP2 specific or control siRNA (Supplementary Fig. S2A). The cells were imaged, and the distribution of the D4H probe between LEs and the PM was quantified by visual inspection of the mCherry-D4H-expressing cells (>300 cells were analyzed).

As reported for HeLa cells, ORP2 KD caused perturbations in the distribution of D4H-accessible cholesterol between endosomes and PM also in HUVECs. In the control cells, the mCherry-D4H cholesterol probe typically distributed to both the LEs and the PM, while in the majority (~60%) of D4H-expressing ORP2 KD cells the D4H-bound pool of cholesterol accumulated into LAMP1-positive late endosomal compartments (Fig. 1A, B). Moreover, the cells depleted of ORP2 showed a significantly reduced distribution of mCherry-D4H to the PM.

Consistently, overexpression of wild type (wt) ORP2-pEGFP-C1 (Supplementary Fig. S2A) in HUVECs shifted the D4H-bound cholesterol towards the PM, seen as significantly increased PM localization of the D4H probe compared to cells transfected with the pEGFP-C1 vector control (Fig.1C, D). Of note, in HUVECs overexpressing either sterol or PIP-binding deficient mutants of ORP2, ORP2(ΔELSK) or ORP2(mHHK) (Supplementary Fig. S2A), respectively, the D4H probe accumulated to late endosomes similar to the ORP2 KD cells (Fig. 1C, D), suggesting a crucial role for both sterol and PIP-binding in the ORP2-mediated cholesterol redistribution.

Cholesterol content in plasma membranes isolated from the control and ORP2 KD cells was measured with Amplex Red assay. These experiments did not reveal a significant reduction of the PM total cholesterol content in the ORP2 KD HUVECs, albeit the mean measured for the KD cells showed a reducing trend (Fig.

2A). We next assayed the interaction of the cholesterol probe His_6-ALOD4 with the mobile extracellular leaflet cholesterol in the KD and control cells. Similar to the PM total cholesterol measurement, no difference was observed in the association of the probe with cell surfaces on ORP2 KD and control cells, while extraction of PM cholesterol with MβCD strongly reduced the cellular association of the probe (Fig. 2B). These observations suggest that the impact of ORP2 depletion may rather affect the PM cholesterol organization than its bulk amount in HUVECs.

ORP2 controls the PM PI(4,5)P_2 content

As ORP2 was reported to act as an exchange-type 'countercurrent transporter' of cholesterol and PI(4,5)P_2 (17), we quantified the PI(4,5)P_2 concentration in the inner leaflet of the PM of HUVECs in the absence or presence of ORP2 KD using the epsin 1 ENTH domain as a PI(4,5)P_2 sensor. As observed with other mammalian cell lines (20-22), HUVECs showed a spatially heterogeneous distribution of PI(4,5)P_2 in the inner leaflet of the PM (Fig. 2C). The spatially averaged concentration was 0.30 ± 0.10 mol% and remained essentially constant for at least 10 min. This value is significantly lower than that observed with several cell lines, such as NIH 3T3 (20-22), which may suggest a lower basal level of PI(4,5)P_2-dependent activities at the PM of the resting primary HUVECs than in transformed cell lines. The ORP2 KD caused ca. 2.5-fold increase (i.e., to 0.75 ± 0.09 mol%) in the spatially averaged PM concentration of PI(4,5)P_2, consistent with the view that ORP2 indeed transfers PI(4,5)P_2 to the internal membrane organelles in exchange for cholesterol.

The PM PI(4,5)P_2 content of the ORP2 KD and control HUVECs was also measured biochemically. We isolated the PM of the cells, then extracted the PM lipids and subsequently measured the PI(4,5)P_2 content by utilizing a competitive PI(4,5)P_2 ELISA assay (Echelon Biosciences). The results showed significantly increased PI(4,5)P_2 concentrations for ORP2 KD PM samples as compared to the controls (Fig. 2D), validating the results obtained from the PI(4,5)P_2 probe assay.

ORP2 overexpression enhances protrusion formation in HUVECs

We recently showed that ORP2 localized to cortactin-positive lamellipodia and enhanced polarized cell protrusions when overexpressed in HuH7 hepatoma cells

(10). Here, we examined whether ORP2 overexpression has similar effects on primary endothelial cells. In accordance with our previous report, we found that ORP2 enhanced protrusion formation also in HUVECs (Fig. 3A, B). A majority (86%) of the cells expressing ORP2(wt) presented with prominent PM protrusions, whereas only less than 30% of the GFP-expressing control cells showed protrusions under the basal culture conditions (Fig. 3B). Interestingly, the ORP2-mediated enhancement in protrusion formation seemed to depend on ORP2's ability to bind both sterols and PIPs, since the ORP2(ΔELSK) and ORP2(mHHK) mutants were unable to provoke PM protrusions (Fig. 3B).

ORP2 KD inhibits angiogenic tube formation *in vitro*

Efficient cholesterol trafficking and protrusion formation are crucial for EC sprouting and angiogenesis. Since ORP2 had drastic effects on both of these cellular processes, we assessed the possible effect of ORP2 on angiogenic tube formation *in vitro*. ORP2 was depleted from HUVECs by lentiviral transduction and the tube forming ability of the transduced cells was studied by seeding them on a matrix supplemented with endothelial growth factors. The cells were imaged at five hours after seeding, and the tube formation parameters were analyzed from images. ORP2 KD drastically inhibited the formation of the EC tubular network (Fig. 3C, D). For example, the number of tubule nodes and junctions were both reduced by approximately 70%, the number of meshes and tube segments by over 80%, the number of branching points by 46%, and total branch length by 83% as compared to control HUVECs. Of note, the angiogenesis inhibitory effect of ORP2 KD was partly rescued when the cells were loaded with external cholesterol by 3-hour incubation with MβCD-cholesterol complex (Fig. 3C, D). In the control cells, however, similar cholesterol loading inhibited the angiogenic tube formation, underscoring the importance of a physiologic cholesterol content or organization for the process (Fig. 3C, D).

ORP2 KD alters the gene expression profiles of multiple angiogenic pathways

To study whether the angiogenic defects of ORP2 KD HUVECs are associated with changes of the transcriptome, we performed a next-generation RNA sequencing (RNAseq) of the lentivirally transduced ORP2 KD HUVECs. The differential RNAseq analysis revealed significantly (Log2 fold change > 1) altered mRNA

profiles for more than 1000 genes as compared to the control shRNA-transduced HUVECs. Interestingly, by utilizing the ConsensusPathDB gene set over-representation tool (28) to assess the affected signaling pathways in the ORP2-depleted HUVECs, we found significantly (adjusted $p<0.05$) altered gene expression in several pathways associated with angiogenesis (Table 1). Strikingly, the VEGF-VEGFR2 pathway was the single most significantly affected signaling pathway in the ORP2 KD HUVECs, with as many as 76.7% of either up- or downregulated overlapping gene IDs (Table 1, Supplementary Fig. S3A). In addition, pathways related to e.g. Rho GTPase, epidermal growth factor receptor (EGFR), focal adhesion kinase (FAK), Notch, mammalian target of rapamycin (mTOR), hypoxia inducible factor-1-α (HIF-1-α), phosphoinositide 3 kinase/protein kinase B (PI3K/Akt), and mitogen activated protein kinase (MAPK) signaling were among the angiogenic signaling pathways affected in the ORP2-depleted cells (Table 1). Moreover, a number of angiogenesis-initiating cellular functions downstream of the prementioned signaling pathways such as 'cell proliferation', 'cytoskeleton organization', 'cell motility' and 'cell adhesion', were predicted to be affected in the ORP2 KD HUVECs by gene ontology (GO) analysis (Supplementary Table S2). Consistently, also angiogenesis itself, alongside with e.g. 'vasculature development', 'tube morphogenesis' and 'blood vessel remodeling' were predicted as significantly affected biological processes in the ORP2 KD HUVECs (Table 2).

ORP2 KD alters the expression of several genes regulating cholesterol homeostasis and plasma membrane lipid organization

To assess the mRNA alterations in ORP2 KD HUVECs putatively responsible for the defects in cholesterol transport, the RNAseq data was searched for significantly affected signaling pathways and cell functions associated with cholesterol homeostasis and transfer. The ConsesusPathDB analysis uncovered the major cholesterol homeostasis coordinating pathway, 'sterol regulatory element-binding protein (SREBP) signaling', as one of the most significantly affected signaling pathways in ORP2 KD cells, with 80.9% of overlapping genes (see full list of significantly affected SREBP target genes in Supplementary Table S3). In addition, processes such as 'sterol biosynthesis and metabolism', 'LDL particle clearance' and

'cholesterol storage' were among the significantly affected cellular functions predicted by the ConsensusPathDB GO analysis (Table 3).

As ORP2 is suggested to transport cholesterol towards the PM, we wondered whether the expression of genes regulating PM cholesterol-rich raft domains was altered in ORP2 KD HUVECs. Since lipid raft-associated proteins as a category are not included in the pathway databases used (Wikipathway, KEGG, Reactome and PID), we ran a separate comparison of the ORP2 KD RNAseq data against the RaftProt database (31), available at http://raftprot.org. The analysis revealed that 69.4% of the gene IDs found in the RaftProt database were significantly affected in ORP2 KD HUVECs. Moreover, 'PM organization', 'membrane raft organization', and 'membrane raft assembly' were among the significantly enriched GO terms in the ConsensusPathDB analysis (Table 3).

ORP2 regulates the activity of VEGFR2 and several of its downstream targets

Encouraged by the RNAseq analysis suggesting 'VEGF-VEGFR2 signaling' as the most significantly affected pathway in OPR2 KD HUVECs, the activity of this pathway and its major regulatory nodes was studied by western blot analysis. HUVECs were stimulated with VEGF-A_{165} for 0, 3, or 12 min and the phosphorylation of VEGFR2(Tyr1175), Akt(Ser473), p70S6 kinase(Thr398), a marker for mTOR activity, ERK1/2(Thr202/Tyr204), eNOS(Ser117) and FAK(Tyr397) were detected by the respective phospho-specific antibodies. These angiogenic effectors are responsible for mediating extracellular angiogenic signal transduction (VEGFR2), cell survival and energy metabolism (Akt, mTOR), cell proliferation (ERK1/2), nitric oxide production and cell permeability (eNOS), and cell adhesion and migration (FAK). The analysis uncovered that the ORP2 KD resulted in a decreased activating phosphorylation of the 230-kDa VEGFR2 at both the 3-min and the 12-min time points of the VEGF stimulus (Fig. 4A). Quantification of the 12-min time point showed a drastic 59% ± 11% reduction in the phospho-VEGFR2 signal in the ORP2 KD cells as compared to control (the phospho-antibody signal was normalized by the total protein signals of the respective samples, Supplementary Fig. S2B). Moreover, ORP2 KD resulted in a significant inhibition of the activating phosphorylation of VEGFR2 downstream targets Akt (−46 ± 5%), eNOS3 (−50 ± 8%), and p70S6K (−31 ± 7%) upon 12-min VEGF stimulus as compared to the

controls (Fig. 4B, Supplementary Fig. S2C). There was no significant difference in the activating phosphorylation of FAK, and changes in the activity of ERK1/2 were inconsistent (data not shown). Of note, PM cholesterol depletion mediated by MβCD decreased the activity of VEGFR2, Akt, eNOS, and p70S6K similarly to ORP2 KD upon 12-min VEGF stimulus (Fig. 4C, Supplementary Fig. S2C).

ORP2 KD decreases the expression of Caveolin-1 and VE-cadherin

The mRNA sequencing (RNAseq) data of ORP2 KD cells revealed downregulation of several genes encoding raft-associated proteins. Among these were proteins such as Caveolin-1, Flotillin-1, Annexin A2 and vascular endothelial cadherin (VE-cadherin). To assess the effects of ORP2 KD on these raft components at the protein level, we compared their expression levels between ORP2 KD and control cells by western blot. The immunodetection revealed that the expression of Caveolin-1, a major structural component of caveolae, and VE-cadherin, a mediator of cell-cell contacts, were significantly decreased in ORP2 KD HUVECs (−58 ± 3% and −65 ± 18%, respectively) as compared to control levels (Fig. 4D), suggesting alterations in PM caveolae or lipid rafts. The expression levels of Flotillin-1 and Annexin A2, however, remained unchanged between ORP2 KD and control cells (Fig. 4E).

ORP2 KD impairs several angiogenic cell functions

GO analysis of the ORP2 KD RNAseq data predicted several angiogenic cell functions downstream of VEGF signaling, such as ‘cell cycle’, ‘cell migration’ and ‘actin cytoskeleton organization’ to be significantly modified in ORP2-depleted HUVECs (Supplementary Table S2). We therefore tested whether these cell functions were altered in the ORP2 KD HUVECs.

To determine the effects of ORP2 KD on cell proliferation and survival, we employed (i) a microelectrode-based xCELLigence® real-time cell analysis system and (ii) a viability assay based on the enzymatic reduction of the tetrazolium salt MTT by metabolically active cells. ORP2 KD reduced the xCELLigence® proliferation signal by 44.7% ± 6.6% (at a 12-h time point) as compared to HUVECs transduced with non-target control virus (Fig. 5A). Consistently, in the MTT viability assay the ability of VEGF-A_{165} (50 ng/ml) to stimulate EC survival after a 12-h incubation was significantly decreased (−40.7 ± 8.0%) in the HUVECs transduced with shORP2 lentivirus compared to the controls (Fig.5B).

One of the most affected cellular functions in the RNAseq of ORP2 depleted HUVECs was cell mobility and migration. We therefore studied the migration capacity of ORP2 KD HUVECs by (i) planar wound healing assays and (ii) a real-time xCELLigence® trans-filter migration application. These independent methods revealed impaired ability for ORP2-depleted ECs to migrate under basal and growth-factor-stimulated conditions, respectively (Fig. 5C-E). The wound closure of ORP2 KD HUVECs showed 40.9% ± 25.2% reduction under basal growth conditions as compared to the control cells (Fig. 5C,D). Consistently, the directed trans-filter migration of ORP2 KD cells was inhibited by 44.4% ± 19.5% as compared to control HUVECs in the xCELLigence® analysis (Fig. 5E).

The effects of ORP2 KD on overall cell morphology and shape were assessed by observing the cells under a bright-field microscope. ORP2 KD HUVECs typically had an elongated and spread-out cell shape distinct from the controls (Fig. 5F). Analysis of cell dimensions of the ORP2 KD and control cells showed a significant increase (+42.2% ± 7.7%) in surface area covered by an individual ORP2 KD cell as compared to a control cell, suggesting increased spreading of the KD cells on the substratum. To study the effects of ORP2 KD on cytoskeletal morphology in HUVECs, the cells were stained with Oregon green phalloidin to visualize F-actin stress fibers. Interestingly, ORP2 KD promoted the formation of an abnormal actin stress fiber morphology: The fibers/fiber bundles were thicker and more co-aligned than in the control cells (Fig. 5G). Immunostaining of active focal adhesions of ORP2 KD and control HUVECs by anti-phospho-paxillin revealed an altered, aligned distribution also for focal adhesions in the ORP2 KD cells (Fig. 5G). Together, these observations imply that in endothelial cells ORP2 KD results in an altered cytoskeletal morphology and cell anchoring to the substratum, as predicted by the GO analysis of RNAseq results.

ORP2 protein interactome overlaps with the VEGFR signaling pathway and the lipid raft proteome

To further characterize the molecular mechanisms by which ORP2 affects EC homeostasis, we carried out a pull down-based mass spectrometric analysis of ORP2 binding partners in HUVECs. The analysis revealed 464 proteins that were enriched >5 fold in the ORP2-2xStrep sample as compared to the negative control (a full list of

ORP2-2xStrep interactome in HUVECs in avaiulanble upion request from the authors). Intriguingly, the ConsensusPathDB analysis of the ORP2 interactome revealed VEGF-VEGFR2 signaling as one of the most significant ($p=1.65^{-08}$) angiogenic pathways with several overlapping gene IDs, consistent with the findings of the ORP2 KD RNAseq data. Other angiogenic signaling pathways shared between the ORP2 KD RNAseq data and the ORP2 interactome were e.g. Rho GTPase, TGF-β, EGF-EGFR, PDGFR-β, FAK, PI3K/Akt, HIF-1-α and MAPK signaling (Table 1). In addition, many of the angiogenic cell functions downstream of VEGFR2 and predicted to be affected in the RNAseq data were included also in the GO hits of the interactome data. For example, 'cell cycle', 'cytoskeleton organization', 'cell motility' and 'cell adhesion' overlapped in both of these independent data sets, suggesting that a major part of these observations reflect specific ORP2 functions. Of note, also 'vasculature development', 'tube morphogenesis and development', 'sprouting angiogenesis' and 'cellular response to hypoxia' were among the GO terms shared between the ORP2 KD RNAseq and the interactome data. Moreover, 328/464 (70.7%) of the identified interaction partners of ORP2 overlapped with the lipid raft-associated proteins listed in the RaftProt database. Intriguingly, most of the putative interaction partners of ORP2 that were associated with the VEGF-VEGFR2 pathway were reported to be associated also with lipid rafts by the RaftProt database (Supplementary Fig. S3B), supporting a connection between the ORP2 regulation of angiogenic tube formation and cholesterol-enriched PM domains.

ORP2 KD reduces compartmentalization of VEGFR2 to the buoyant lipid raft membrane fractions

VEGFR2 is associated with PM lipid rafts, a location shown to be of importance in regulating the activity of the receptor (3, 6). To study the mechanism by which ORP2 contributes to VEGFR2 activity, we assessed by detergent-free cell fractionation whether ORP2 KD affected the association of VEGFR2 with HUVEC raft domains. The membrane fractionation experiments showed a marked reduction in the relative abundance of VEGFR2 in the buoyant lipid raft-fraction (fraction 4) in the ORP2 KD HUVECs compared to the control cells (Fig. 6A, B), suggesting that the depletion of ORP2 causes a redistribution of VEGFR2 away from the buoyant raft membrane domains. As the lipid raft-association of VEGFR2 has been previously shown to be dependent on the PM cholesterol content (3, 6), we next analyzed the amount of

cholesterol in the ORP2 KD membrane fractions. This analysis revealed a significant reduction in the relative concentration of cholesterol in the lipid raft fraction (fraction 4) of ORP2 KD cells as compared to the control, while the cholesterol content of the heavier membrane fractions 5 & 6 significantly increased in the ORP2 KD cells as compared to the control (Fig. 6C).

ORP2 KD increases VEGF receptor cleavage at the PM

To further study the effects of ORP2 KD on the PM-associated VEGFR2 we performed surface receptor biotinylation assays to isolate the PM pool of the receptor. Interestingly, ORP2 KD significantly increased the portion of PM-associated C-terminal 130 kDa cleaved residue of the biotinylated VEGFR2 as compared to control cells (Fig. 6D, E). Notably, the 130 kDa residue was nearly invisible in the intracellular pool of the VEGFR2, suggesting that the cleavage occurred specifically at the cell surface (Fig. 6D). VEGFR2 has been reported to be cleaved at the PM by TNFα-converting enzyme (TACE or ADAM17), a matrix metalloproteinase (MMP) sequestered in lipid rafts (32, 33). To examine whether the increased VEGFR2 cleavage at the PM of ORP2 KD cells is catalyzed by MMPs, we treated the cells with 5 μM Marimastat, an MMP inhibitor, and repeated the biotinylation assay. Interestingly, the Marimastat treatment completely abolished the 130 kDa cleaved form of VEGFR2 in the ORP2 KD cells (and in the controls) (Fig. 6F), demonstrating that the enhanced VEGFR2 cleavage upon ORP2 depletion is due to increased susceptibility of the receptor to MMPs.

To confirm that the VEGFR2 cleavage is specific for changes in ORP2 expression, we lentivirally overexpressed the wild type ORP2 in HUVECs and checked whether it had an effect on generation of the 130 kDa VEGFR2 residue. Interestingly, the overexpression of ORP2 significantly alleviated the VEGR2 cleavage, confirming that the cleavage of VEGFR2 at the PM was indeed modulated by the availability of ORP2 (Fig. 6G).

The shedding by ADAM17 of its substrates has been shown to depend on the PM raft cholesterol (33, 34). Therefore, we next assessed whether the increase in MMP-mediated VEGFR2 cleavage upon ORP2 KD could be due to a modification of PM cholesterol organization. To this end, we depleted cholesterol from the PM of untransduced HUVECs by a time series of MβCD incubations and repeated the

receptor biotinylation assay. Intriguingly, a time-dependent increase in the 130 kDa residue of VEGFR2 was observed at the PM of the cholesterol depleted cells (Fig. 6H), suggesting cholesterol-dependency of the receptor shedding. Moreover, also this MβCD-mediated increase in VEGFR2 shedding at the PM could be rescued by Marimastat treatment.

As VEGFR2 shedding by MMPs releases the N-terminal VEGF-binding domain of the receptor, we wondered whether the receptor cleavage upon ORP2 KD could be the cause for the reduced phosphorylation of the 230 kDa receptor in the PM of the KD cells. To test this hypothesis, we again treated the ORP2 KD cells with Marimastat o/n, stimulated them with VEGF-A for 12 min and detected the VEGFR2 phosphorylation by western blot. The reduction in the phosphorylation of VEGFR2 in the ORP2 KD cells was completely rescued by the Marimastat treatment (Fig 6I). These data, together with the above cell fractionation observations suggest that the primary mechanism by which ORP2 modulates VEGFR cleavage and phosphorylation at the PM is via alterations in the PM cholesterol organization, resulting in a redistribution of VEGFR2 to a location where it is sensitized to MMP activity. The reduced phosphorylation of the 230-kDa VEGFR2 is, according to our data, secondary to proteolytic cleavage of a receptor pool at the PM.

ORP2 KO interferes with retinal vasculature development in vivo in mice

To investigate whether the lack of ORP2 interferes with angiogenesis *in vivo*, we generated global Osbpl2 KO mice by deleting the Osbpl2 exon 3 by CRISPR/Cas9-mediated gene targeting. This resulted in viable and superficially healthy animals with an allele encoding a truncated Osbpl2 protein spanning only the first 31 aa residues of the protein. Western blot analysis of the brain of the animals verified a lack of immunoreactive Osbpl2 protein in the Osbpl2$^{-/-}$ animals and an approximately 50% reduction in the heterozygotes (Supplementary Fig. S1). We then imaged the microvasculature in the retina by isolectin B4 staining of post-natal day 7 Osbpl2 (ORP2) knock-out and littermate control mice. This revealed a subtle but significant alteration of morphology characterized by reduced vessel length and increased density of tip cells and perpendicular sprouts in both the front and the central areas of the retinal vasculature (Fig. 7A-D). The increase of tip cells and sprouts suggested a possible disturbance of Notch signaling. Consistent with this notion the qPCR

analysis of retina revealed significantly reduced mRNA expression of the Notch pathway components Cyclin D1 (CCND1), Delta-like 1 (DLL1), Jagged 1 (JAG1) and signal transducer and activator of transcription 1 (STAT1) (Fig. 7E). Of note, also in the RNAseq of ORP2 KD HUVECs the Notch pathway was significantly affected (Table 1), and the above four genes dampened in the Osbpl2$^{-/-}$ mouse retina were consistently downregulated in the HUVEC model (Fig. 7E). Importantly, analysis of retinal mRNA expression levels also revealed a significant down-regulation of Cdh5 (VE-cadherin) as well as of top cholesterol biosynthetic genes suppressed in the HUVEC model, Fdft1 and Srebp-2 (p=0.06), as well as mTOR, a hub involved in VEGF, Notch and SREBP signaling (35-37). These observations lend support to the notion that cholesterol homeostasis, VE-cadherin dependent EC adhesion and intercellular Notch signaling are affected in both the HUVEC model and in ORP2 KO mice *in vivo*.

DISCUSSION

In the present study we report a crucial functional role of the intracellular cholesterol and PI(4,5)P_2 transporter ORP2 in endothelial cells, a cell type playing decisive roles in common diseases such as cardiovascular diseases, type 2 diabetes and cancers. We show in primary human endothelial cells that ORP2 knock-down, or the overexpression of its mutants defective in sterol or phosphoinositide binding, alter the subcellular distribution of cholesterol as detected with the D4H probe, and demonstrate that ORP2 manipulations affect the formation of HUVEC surface protrusions in a ligand-dependent manner. As a key finding we show that ORP2 KD in HUVECs inhibits angiogenesis *in vitro* in a tube-forming assay and its loss *in vivo* in a knock-out mouse model results in a subtle alteration of retinal angiogenesis. Consistent with the above observations, RNA sequencing revealed that ORP2 knock-down in HUVECs induced significant changes in the gene expression of multiple angiogenic pathways and cell functions. Our data also demonstrates that ORP2 KD attenuates the migration and proliferation capacity of HUVECs and impairs their viability. As key mechanistic observations we show impaired VEGF signaling in HUVECs subjected to ORP2 KD, featured by defective activating phosphorylation of

VEGFR2, Akt, eNOS, and p70S6K. We further demonstrate that ORP2 depletion reduces cholesterol in the buoyant lipid raft domains, shifts VEGFR2 away from these domains, induces enhanced proteolytic cleavage of VEGFR2 by MMPs and dampens expression of the raft-associated proteins Caveolin 1 and VE-cadherin, consistent with the view that ORP2 KD disturbs cholesterol-dependent functional domains at the EC plasma membrane.

VEGFR2 signaling and angiogenesis are thought to require distribution of the receptor into lipid rafts. Liver X receptor activation inhibits angiogenesis through enhancement of cholesterol efflux resulting in the removal of VEGFR2 from raft domains (3). Consistently, acceleration of cholesterol efflux to high-density lipoproteins by the apoA-I binding protein (AIBP) interferes with the raft association of VEGFR2 and inhibits angiogenesis *in vitro* in HUVECs and *in vivo* in zebrafish (6). Moreover, blockade of cholesterol transport through endo-lysosomal compartments in HUVECs by the pharmaceuticals itraconazole, astemizole or cepharantine inhibits angiogenesis (5, 8, 38, 39). The present findings of ORP2 KD-associated disturbances in cholesterol distribution in HUVECs are in agreement with these earlier observations.

Of the ligands of ORP2, not only cholesterol plays a key role in angiogenesis, but also PI(4,5)P_2, which we show to be enriched in the PM of ORP2-depleted HUVECs, is pivotal for the process. It acts as a substrate for phosphoinositide 3-kinase (PI3K) and phospholipase Cγ (PLCγ). PI3K plays central roles in angiogenesis via effectors such as Akt and FOXO (40-43), while PLCγ acts downstream of VEGF and is crucial for vasculogenesis (41, 44, 45). Of note, excess of PI(4,5)P_2 at the endothelium has been reported to promote increased angiogenesis *in vivo* in zebrafish (46).

ORP2 was previously reported to promote cholesterol delivery to the PM in exchange for PI(4,5)P_2 in HeLa cells (17). Consistently, we observed in HUVECs subjected to ORP2 KD an increase of PM PI(4,5)P_2, whereas no significant reduction of PM total cholesterol content was detected, in apparent contradiction with the data of Wang et al. The reasons for this most likely lie in the use of different cell systems (HeLa vs. HUVECs) and different genetic manipulations (complete CRISPR-mediated knock-out vs. partial KD by RNA interference). We do not find this surprising, since cholesterol is a major constituent of the PM, the homeostasis of

which is secured by multiple mechanisms which may vary between cell types and cancerous vs. primary cells (47, 48). Interference with ORP2 resulted in the accumulation of the D4H cholesterol probe in LE in both HeLa cells (16) and HUVECs (present study), which could indicate an altered organelle cholesterol concentration or reflect an altered organization of the cholesterol affecting its probe accessibility. It should also be noted that overexpression of ORP2 was earlier shown to enhance the transport of newly synthesized cholesterol from the ER to the PM (13). RNA sequencing of ORP2 KD HUVECs revealed a significant reduction in the expression of SREBP target genes, and parallel observations were made in the retina on Osbpl2$^{-/-}$ mice, consistent with the view that ORP2 depletion may result in an elevation of cholesterol concentration in ER membranes harbouring the SREBP-SCAP-INSIG apparatus (49, 50). The observations in this study do not allow us to state with certainty which specific step of inter-organelle cholesterol transport ORP2 mediates in ECs.

The present data demonstrate downstream signaling effects of ORP2 KD in several branches of the VEGF-VEGFR2 signaling network. In this context it is, however, important to notice that activity of the VEGFR2 downstream components analyzed, Akt, eNOS and p70S6K (mTOR target) is also sensitive to the availability of PM cholesterol (as this study demonstrates) and is reported to be regulated by their raft association (51-53). The suppression of their activity may thus also arise through mechanisms independent of VEGFR2 activity.

A further clue to the mechanism through which ORP2 depletion impairs VEGFR2 function is provided by the observation of enhanced proteolytic cleavage of the receptor in HUVECs, yielding a residual 130-kDa receptor fragment that remains in the PM. This cleavage has been reported to mediate shedding of the receptor from the PM surface, resulting in its inactivation (54). Cell surface biotinylation in the present study confirmed that the cleavage in ORP2-depleted HUVECs occurs at the PM and is mediated by MMPs. Importantly, the VEGFR2 integrity seemed to be susceptible to the PM cholesterol composition, as similar MMP-mediated cleavage was seen in HUVECs with PM cholesterol depleted by using MβCD. The impaired activating phosphorylation and enhanced proteolytic cleavage upon ORP2 KD may thus be due to a disturbance of the PM domain organization and the lateral distribution of VEGFR2, a notion supported by our observation that ORP2 KD shifts

VEGFR2 away from buoyant raft membranes. Of note, no significant reduction of total cellular VEGFR2 was observed in the ORP2 KD cells, but the effect was selective for the receptor pool biotinylated at the PM.

We have previously shown that ORP2 knock-out in HuH7 hepatoma cells results in defective cell migration, proliferation and F-actin morphology (10), and impairs Akt activation, glucose metabolism and triglyceride synthesis (10, 11). There is also evidence for physical interactions of ORP2 with several F-actin regulatory proteins such as IQGAP1, Hsp90 and Cdc37, suggesting that the mechanisms of ORP2 action are not limited solely to inter-organelle lipid transport (10, 11, 15). The present observations on impaired HUVEC migration, proliferation and altered F-actin organization are in line with the previous findings in hepatoma cells (10). While these defects in ORP2-depleted cells could be in part due to loss of protein-protein interactions, they may also reflect defective lipid raft-dependent signaling or PIP homeostasis, especially since $PI(4,5)P_2$ enriched in the PM of ORP2 KD cells plays a key role in cortical F-actin regulation (55, 56).

The retinal phenotype of the Osbpl2$^{-/-}$ animals suggests that, in apparent contrast to the HUVEC data, no physiologically significant inhibition of VEGFR2 signaling is manifested *in vivo*, since such defects result in drastic disturbances of angiogenesis (57, 58). If the VEGFR2 signaling, nevertheless, is affected in the animals, this could be compensated *in vivo* by as yet undefined mechanisms, such as enhanced activity of VEGFR3, which has the capacity to sustain angiogenic sprouting and vascular network formation during development (57, 58). The increased density of tip cells and sprouts of the Osbpl2$^{-/-}$ vasculature would be consistent with Notch signaling being affected (59, 60). The Notch pathway dampens the tip cell phenotype in stalk cells in the vicinity of an initial tip cell, thus allowing each tip cell to efficiently lead the growth of a branch, resulting in a normal vascular network structure (61). Of note, the organization of PM rafts is reported to affect Notch activity also independent of VEGF signaling (62). Despite the obvious inconsistently of the *in vitro* and *in vivo* observations concerning VEGFR2 signaling, gene expression analyses of the ORP2$^{-/-}$ mouse retina revealed interesting parallels between the *in vitro* and *in vivo* data: The Cdh5 (VE-cadherin) mRNA was significantly reduced in the Osbpl2$^{-/-}$ retina, similar to the HUVEC model, and the top cholesterol biosynthetic gene suppressed in the ORP2 KD HUVECs, Fdft1, as well as Srebp-2 and mTOR were downregulated. Moreover, the Notch pathway genes Ccnd1, Dll1,

Jag1 and Stat1 were found suppressed in both the ORP2$^{-/-}$ mice and the HUVEC subjected to ORP2 KD.

VE-cadherin dynamics plays a crucial role in the inter-cellular contacts at which Notch signals are mediated (63-65). VE-cadherin is also reported to stabilize VEGFR2 (66), consistent with our observation of coincident VE-cadherin reduction and VEGFR2 cleavage. Moreover, depletion of VE-cadherin increases angiogenic sprouting (63, 67), in agreement with our data showing an increase of tip cells and perpendicular sprouts in ORP2$^{-/-}$ retina. Puzzlingly, the retinal phenotype of the ORP2$^{-/-}$ animals is very subtle, although the PM cholesterol organization is reported to have major effects on VEGF signaling and angiogenesis (3,5,6,8,31,32). A plausible explanation is the existence of several overlapping cholesterol trafficking routes from endosomes to the PM, such as a Rab8-myosin V-mediated vesicular pathway (68) and a recently described ORP1S-mediated pathway (69). Generation and characterization of an endothelial-specific knock-out of Osbpl2 in the future will be required to reach a detailed understanding of Osbpl2/ORP2 function in the biology of ECs.

To conclude, the present work documents for the first time a function of an OSBP-related lipid transfer protein in angiogenesis. While the molecular details are as yet not completely understood, our data suggest that ORP2 activity is required for normal angiogenic signaling, the underlying mechanism most likely involving the impacts of ORP2 on the PM lipid composition and/or domain organization. The present work prompts further research to elucidate the functions of lipid transfer proteins in healthy ECs and in diseases involving endothelial dysfunction.

ACKNOWLEDGMENTS

We thank Prof. Gregory Fairn (Department of Biochemistry, University of Toronto, ON, Canada) for kindly providing the fluorescent D4H construct, Prof. Arun Radhakrishnan (Univ. of Texas Southwestern Medical Center, Dallas, TX) for kindly providing the purified His_6-ALOD4 protein, Prof. Pipsa Saharinen (Faculty of Medicine, Univ. of Helsinki and the Wihuri Research Institute, Helsinki, Finland) for generous help and advice on the EC work, and Adj. prof. You Zhou (Cardiff University School of Medicine, Cardiff, UK) for kind support in pathway analysis. We also acknowledge the invaluable help of Biomedicum Imaging Unit (BIU; Helsinki Institute of Life Science, HiLIFE, and Biocenter Finland imaging

infrastructure), the Biomedicum Functional Genomics Unit (FUGU; HiLIFE), and the Genome Biology Unit (GBU), part of the Genome Editing and Stem Cells (GoEditStem) core-unit platform and of the National Biocenter Finland Genome-wide methods network (GWM). This study was supported by grants from the Academy of Finland (grants 285223 and 322647 to V.M.O. and 282192 and 324929 to E.I.), the Sigrid Juselius Foundation, the Magnus Ehrnrooth Foundation, the Finnish Foundation for Cardiovascular Research (V.M.O.), the Leducq Foundation for Cardiovascular Research (E.I.), the Emil Aaltonen Foundation (A.Ko.), the Ida Montin Foundation (A.Ko.), the National Institutes of Health (R35GM122530 to W.C.) and the NSFC, China (grants 8170438 and 91439122 to D.Y.). The funding bodies played no role in the study design, analysis or interpretation of the data, writing of the report or the decision to submit the article for publication.

AUTHOR CONTRIBUTIONS

A.Ko., G. P., A.Ki, R.K., A.A., J.T., A.R., O.K. and J.N. performed the experiments. A.Ko., A.Ki, A.A., E.I., W.C., D.Y. and V.M.O. designed the experiments and interpreted the results. A.Ko. and V.M.O wrote the manuscript and all authors commented on it.

CONFLICT OF INTEREST

The authors declare no conflict of interest concerning this study.

REFERENCES

1. Lingwood, D., and Simons, K. (2010) Lipid rafts as a membrane-organizing principle. *Science* **327**, 46-50
2. Anderson, R. G. (1998) The caveolae membrane system. *Annu Rev Biochem* **67**, 199-225
3. Noghero, A., Perino, A., Seano, G., Saglio, E., Lo Sasso, G., Veglio, F., Primo, L., Hirsch, E., Bussolino, F., and Morello, F. (2012) Liver X receptor activation reduces angiogenesis by impairing lipid raft localization and

signaling of vascular endothelial growth factor receptor-2. *Arterioscler Thromb Vasc Biol* **32**, 2280-2288

4. Zhu, L., and Fang, L. (2015) AIBP: A Novel Molecule at the Interface of Cholesterol Transport, Angiogenesis, and Atherosclerosis. *Methodist Debakey Cardiovasc J* **11**, 160-165
5. Lyu, J., Yang, E. J., Head, S. A., Ai, N., Zhang, B., Wu, C., Li, R. J., Liu, Y., Chakravarty, H., Zhang, S., Tam, K. Y., Dang, Y., Kwon, H. J., Ge, W., Liu, J. O., and Shim, J. S. (2018) Astemizole Inhibits mTOR Signaling and Angiogenesis by Blocking Cholesterol Trafficking. *Int J Biol Sci* **14**, 1175-1185
6. Fang, L., Choi, S. H., Baek, J. S., Liu, C., Almazan, F., Ulrich, F., Wiesner, P., Taleb, A., Deer, E., Pattison, J., Torres-Vazquez, J., Li, A. C., and Miller, Y. I. (2013) Control of angiogenesis by AIBP-mediated cholesterol efflux. *Nature* **498**, 118-122
7. Cross, M. J., Dixelius, J., Matsumoto, T., and Claesson-Welsh, L. (2003) VEGF-receptor signal transduction. *Trends Biochem Sci* **28**, 488-494
8. Lyu, J., Yang, E. J., Head, S. A., Ai, N., Zhang, B., Wu, C., Li, R. J., Liu, Y., Yang, C., Dang, Y., Kwon, H. J., Ge, W., Liu, J. O., and Shim, J. S. (2017) Pharmacological blockade of cholesterol trafficking by cepharanthine in endothelial cells suppresses angiogenesis and tumor growth. *Cancer Lett* **409**, 91-103
9. Kentala, H., Weber-Boyvat, M., and Olkkonen, V. M. (2016) OSBP-Related Protein Family: Mediators of Lipid Transport and Signaling at Membrane Contact Sites. *Int Rev Cell Mol Biol* **321**, 299-340
10. Kentala, H., Koponen, A., Kivelä, A. M., Andrews, R., Li, C., Zhou, Y., and Olkkonen, V. M. (2018) Analysis of ORP2-knockout hepatocytes uncovers a novel function in actin cytoskeletal regulation. *FASEB J* **32**, 1281-1295
11. Kentala, H., Koponen, A., Vihinen, H., Pirhonen, J., Liebisch, G., Pataj, Z., Kivelä, A., Li, S., Karhinen, L., Jääskeläinen, E., Andrews, R., Meriläinen, L., Matysik, S., Ikonen, E., Zhou, Y., Jokitalo, E., and Olkkonen, V. M. (2018) OSBP-related protein-2 (ORP2): a novel Akt effector that controls cellular energy metabolism. *Cell Mol Life Sci* **75**, 4041-4057
12. Laitinen, S., Lehto, M., Lehtonen, S., Hyvärinen, K., Heino, S., Lehtonen, E., Ehnholm, C., Ikonen, E., and Olkkonen, V. M. (2002) ORP2, a homolog of

oxysterol binding protein, regulates cellular cholesterol metabolism. *J Lipid Res* **43**, 245-255

13. Hynynen, R., Laitinen, S., Käkelä, R., Tanhuanpää, K., Lusa, S., Ehnholm, C., Somerharju, P., Ikonen, E., and Olkkonen, V. M. (2005) Overexpression of OSBP-related protein 2 (ORP2) induces changes in cellular cholesterol metabolism and enhances endocytosis. *Biochem J* **390**, 273-283
14. Zhang, C., Zhang, H., Zhang, M., Lin, C., Wang, H., Yao, J., Wei, Q., Lu, Y., Chen, Z., Xing, G., and Cao, X. (2019) OSBPL2 deficiency upregulate SQLE expression increasing intracellular cholesterol and cholesteryl ester by AMPK/SP1 and SREBF2 signalling pathway. *Exp Cell Res* **383**, 111512
15. Escajadillo, T., Wang, H., Li, L., Li, D., and Sewer, M. B. (2016) Oxysterol-related-binding-protein related Protein-2 (ORP2) regulates cortisol biosynthesis and cholesterol homeostasis. *Mol Cell Endocrinol* **427**, 73-85
16. Koponen, A., Arora, A., Takahashi, K., Kentala, H., Kivela, A. M., Jaaskelainen, E., Peränen, J., Somerharju, P., Ikonen, E., Viitala, T., and Olkkonen, V. M. (2019) ORP2 interacts with phosphoinositides and controls the subcellular distribution of cholesterol. *Biochimie* **158**, 90-101
17. Wang, H., Ma, Q., Qi, Y., Dong, J., Du, X., Rae, J., Wang, J., Wu, W. F., Brown, A. J., Parton, R. G., Wu, J. W., and Yang, H. (2019) ORP2 Delivers Cholesterol to the Plasma Membrane in Exchange for Phosphatidylinositol 4, 5-Bisphosphate (PI(4,5)P2). *Mol Cell* **73**, 458-473 e457
18. Weber-Boyvat, M., Kentala, H., Peränen, J., and Olkkonen, V. M. (2015) Ligand-dependent localization and function of ORP-VAP complexes at membrane contact sites. *Cell Mol Life Sci* **72**, 1967-1987
19. Sigoillot, F. D., Lyman, S., Huckins, J. F., Adamson, B., Chung, E., Quattrochi, B., and King, R. W. (2012) A bioinformatics method identifies prominent off-targeted transcripts in RNAi screens. *Nat Methods* **9**, 363-366
20. Yoon, Y., Lee, P. J., Kurilova, S., and Cho, W. (2011) In situ quantitative imaging of cellular lipids using molecular sensors. *Nat Chem* **3**, 868-874
21. Liu, S. L., Sheng, R., O'Connor, M. J., Cui, Y., Yoon, Y., Kurilova, S., Lee, D., and Cho, W. (2014) Simultaneous in situ quantification of two cellular lipid pools using orthogonal fluorescent sensors. *Angew Chem Int Ed Engl* **53**, 14387-14391

22. Liu, S. L., Wang, Z. G., Hu, Y., Xin, Y., Singaram, I., Gorai, S., Zhou, X., Shim, Y., Min, J. H., Gong, L. W., Hay, N., Zhang, J., and Cho, W. (2018) Quantitative Lipid Imaging Reveals a New Signaling Function of Phosphatidylinositol-3,4-Bisphophate: Isoform- and Site-Specific Activation of Akt. *Mol Cell* **71**, 1092-1104 e1095
23. Endapally, S., Infante, R. E., and Radhakrishnan, A. (2019) Monitoring and Modulating Intracellular Cholesterol Trafficking Using ALOD4, a Cholesterol-Binding Protein. *Methods Mol Biol* **1949**, 153-163
24. Kallio, M. A., Tuimala, J. T., Hupponen, T., Klemelä, P., Gentile, M., Scheinin, I., Koski, M., Käki, J., and Korpelainen, E. I. (2011) Chipster: user-friendly analysis software for microarray and other high-throughput data. *BMC Genomics* **12**, 507
25. Langmead, B., and Salzberg, S. L. (2012) Fast gapped-read alignment with Bowtie 2. *Nat Methods* **9**, 357-359
26. Anders, S., Pyl, P. T., and Huber, W. (2015) HTSeq--a Python framework to work with high-throughput sequencing data. *Bioinformatics* **31**, 166-169
27. Love, M. I., Huber, W., and Anders, S. (2014) Moderated estimation of fold change and dispersion for RNA-seq data with DESeq2. *Genome Biol* **15**, 550
28. Kamburov, A., Pentchev, K., Galicka, H., Wierling, C., Lehrach, H., and Herwig, R. (2011) ConsensusPathDB: toward a more complete picture of cell biology. *Nucleic Acids Res* **39**, D712-717
29. Cox, J., Hein, M. Y., Luber, C. A., Paron, I., Nagaraj, N., and Mann, M. (2014) Accurate proteome-wide label-free quantification by delayed normalization and maximal peptide ratio extraction, termed MaxLFQ. *Mol Cell Proteomics* **13**, 2513-2526
30. Tyanova, S., Temu, T., Sinitcyn, P., Carlson, A., Hein, M. Y., Geiger, T., Mann, M., and Cox, J. (2016) The Perseus computational platform for comprehensive analysis of (prote)omics data. *Nat Methods* **13**, 731-740
31. Mohamed, A., Shah, A. D., Chen, D., and Hill, M. M. (2019) RaftProt V2: understanding membrane microdomain function through lipid raft proteomes. *Nucleic Acids Res* **47**, D459-D463
32. Swendeman, S., Mendelson, K., Weskamp, G., Horiuchi, K., Deutsch, U., Scherle, P., Hooper, A., Rafii, S., and Blobel, C. P. (2008) VEGF-A stimulates

ADAM17-dependent shedding of VEGFR2 and crosstalk between VEGFR2 and ERK signaling. *Circ Res* **103**, 916-918

33. Tellier, E., Canault, M., Rebsomen, L., Bonardo, B., Juhan-Vague, I., Nalbone, G., and Peiretti, F. (2006) The shedding activity of ADAM17 is sequestered in lipid rafts. *Exp Cell Res* **312**, 3969-3980
34. Matthews, V., Schuster, B., Schutze, S., Bussmeyer, I., Ludwig, A., Hundhausen, C., Sadowski, T., Saftig, P., Hartmann, D., Kallen, K. J., and Rose-John, S. (2003) Cellular cholesterol depletion triggers shedding of the human interleukin-6 receptor by ADAM10 and ADAM17 (TACE). *J Biol Chem* **278**, 38829-38839
35. Mungamuri, S. K., Yang, X., Thor, A. D., and Somasundaram, K. (2006) Survival signaling by Notch1: mammalian target of rapamycin (mTOR)-dependent inhibition of p53. *Cancer Res* **66**, 4715-4724
36. Wang, B. T., Ducker, G. S., Barczak, A. J., Barbeau, R., Erle, D. J., and Shokat, K. M. (2011) The mammalian target of rapamycin regulates cholesterol biosynthetic gene expression and exhibits a rapamycin-resistant transcriptional profile. *Proc Natl Acad Sci U S A* **108**, 15201-15206
37. Abhinand, C. S., Raju, R., Soumya, S. J., Arya, P. S., and Sudhakaran, P. R. (2016) VEGF-A/VEGFR2 signaling network in endothelial cells relevant to angiogenesis. *J Cell Commun Signal* **10**, 347-354
38. Xu, J., Dang, Y., Ren, Y. R., and Liu, J. O. (2010) Cholesterol trafficking is required for mTOR activation in endothelial cells. *Proc Natl Acad Sci U S A* **107**, 4764-4769
39. Head, S. A., Shi, W. Q., Yang, E. J., Nacev, B. A., Hong, S. Y., Pasunooti, K. K., Li, R. J., Shim, J. S., and Liu, J. O. (2017) Simultaneous Targeting of NPC1 and VDAC1 by Itraconazole Leads to Synergistic Inhibition of mTOR Signaling and Angiogenesis. *ACS Chem Biol* **12**, 174-182
40. Gerber, H. P., McMurtrey, A., Kowalski, J., Yan, M., Keyt, B. A., Dixit, V., and Ferrara, N. (1998) Vascular endothelial growth factor regulates endothelial cell survival through the phosphatidylinositol 3'-kinase/Akt signal transduction pathway. Requirement for Flk-1/KDR activation. *J Biol Chem* **273**, 30336-30343

41. Davies, E. M., Gurung, R., Le, K. Q., and Mitchell, C. A. (2019) Effective angiogenesis requires regulation of phosphoinositide signaling. *Adv Biol Regul* **71**, 69-78
42. Im, E., and Kazlauskas, A. (2006) Regulating angiogenesis at the level of PtdIns-4,5-P2. *EMBO J* **25**, 2075-2082
43. Hamada, K., Sasaki, T., Koni, P. A., Natsui, M., Kishimoto, H., Sasaki, J., Yajima, N., Horie, Y., Hasegawa, G., Naito, M., Miyazaki, J., Suda, T., Itoh, H., Nakao, K., Mak, T. W., Nakano, T., and Suzuki, A. (2005) The PTEN/PI3K pathway governs normal vascular development and tumor angiogenesis. *Genes Dev* **19**, 2054-2065
44. Liao, H. J., Kume, T., McKay, C., Xu, M. J., Ihle, J. N., and Carpenter, G. (2002) Absence of erythrogenesis and vasculogenesis in Plcg1-deficient mice. *J Biol Chem* **277**, 9335-9341
45. Lawson, N. D., Mugford, J. W., Diamond, B. A., and Weinstein, B. M. (2003) phospholipase C gamma-1 is required downstream of vascular endothelial growth factor during arterial development. *Genes Dev* **17**, 1346-1351
46. Pan, W., Pham, V. N., Stratman, A. N., Castranova, D., Kamei, M., Kidd, K. R., Lo, B. D., Shaw, K. M., Torres-Vazquez, J., Mikelis, C. M., Gutkind, J. S., Davis, G. E., and Weinstein, B. M. (2012) CDP-diacylglycerol synthetase-controlled phosphoinositide availability limits VEGFA signaling and vascular morphogenesis. *Blood* **120**, 489-498
47. Mesmin, B., and Maxfield, F. R. (2009) Intracellular sterol dynamics. *Biochim Biophys Acta* **1791**, 636-645
48. Ikonen, E. (2018) Mechanisms of cellular cholesterol compartmentalization: recent insights. *Curr Opin Cell Biol* **53**, 77-83
49. Brown, M. S., and Goldstein, J. L. (1997) The SREBP pathway: regulation of cholesterol metabolism by proteolysis of a membrane-bound transcription factor. *Cell* **89**, 331-340
50. Chang, T. Y., Chang, C. C., Ohgami, N., and Yamauchi, Y. (2006) Cholesterol sensing, trafficking, and esterification. *Annu Rev Cell Dev Biol* **22**, 129-157
51. Lai, C. J., Cheng, H. C., Lin, C. Y., Huang, S. H., Chen, T. H., Chung, C. J., Chang, C. H., Wang, H. D., and Chuu, C. P. (2017) Activation of liver X

receptor suppresses angiogenesis via induction of ApoD. *FASEB J* **31**, 5568-5576

52. Calay, D., Vind-Kezunovic, D., Frankart, A., Lambert, S., Poumay, Y., and Gniadecki, R. (2010) Inhibition of Akt signaling by exclusion from lipid rafts in normal and transformed epidermal keratinocytes. *J Invest Dermatol* **130**, 1136-1145
53. Tran, J., Magenau, A., Rodriguez, M., Rentero, C., Royo, T., Enrich, C., Thomas, S. R., Grewal, T., and Gaus, K. (2016) Activation of Endothelial Nitric Oxide (eNOS) Occurs through Different Membrane Domains in Endothelial Cells. *PLoS One* **11**, e0151556
54. Basagiannis, D., and Christoforidis, S. (2016) Constitutive Endocytosis of VEGFR2 Protects the Receptor against Shedding. *J Biol Chem* **291**, 16892-16903
55. Hilpelä, P., Vartiainen, M. K., and Lappalainen, P. (2004) Regulation of the actin cytoskeleton by PI(4,5)P2 and PI(3,4,5)P3. *Curr Top Microbiol Immunol* **282**, 117-163
56. Zhang, L., Mao, Y. S., Janmey, P. A., and Yin, H. L. (2012) Phosphatidylinositol 4, 5 bisphosphate and the actin cytoskeleton. *Subcell Biochem* **59**, 177-215
57. Benedito, R., Rocha, S. F., Woeste, M., Zamykal, M., Radtke, F., Casanovas, O., Duarte, A., Pytowski, B., and Adams, R. H. (2012) Notch-dependent VEGFR3 upregulation allows angiogenesis without VEGF-VEGFR2 signalling. *Nature* **484**, 110-114
58. Zarkada, G., Heinolainen, K., Makinen, T., Kubota, Y., and Alitalo, K. (2015) VEGFR3 does not sustain retinal angiogenesis without VEGFR2. *Proc Natl Acad Sci U S A* **112**, 761-766
59. Suchting, S., Freitas, C., le Noble, F., Benedito, R., Breant, C., Duarte, A., and Eichmann, A. (2007) The Notch ligand Delta-like 4 negatively regulates endothelial tip cell formation and vessel branching. *Proc Natl Acad Sci U S A* **104**, 3225-3230
60. Hellström, M., Phng, L. K., Hofmann, J. J., Wallgard, E., Coultas, L., Lindblom, P., Alva, J., Nilsson, A. K., Karlsson, L., Gaiano, N., Yoon, K., Rossant, J., Iruela-Arispe, M. L., Kalen, M., Gerhardt, H., and Betsholtz, C.

(2007) Dll4 signalling through Notch1 regulates formation of tip cells during angiogenesis. *Nature* **445**, 776-780

61. Potente, M., and Carmeliet, P. (2017) The Link Between Angiogenesis and Endothelial Metabolism. *Annu Rev Physiol* **79**, 43-66
62. Mao, R., Meng, S., Gu, Q., Araujo-Gutierrez, R., Kumar, S., Yan, Q., Almazan, F., Youker, K. A., Fu, Y., Pownall, H. J., Cooke, J. P., Miller, Y. I., and Fang, L. (2017) AIBP Limits Angiogenesis Through gamma-Secretase-Mediated Upregulation of Notch Signaling. *Circ Res* **120**, 1727-1739
63. Gaengel, K., Niaudet, C., Hagikura, K., Lavina, B., Muhl, L., Hofmann, J. J., Ebarasi, L., Nystrom, S., Rymo, S., Chen, L. L., Pang, M. F., Jin, Y., Raschperger, E., Roswall, P., Schulte, D., Benedito, R., Larsson, J., Hellstrom, M., Fuxe, J., Uhlen, P., Adams, R., Jakobsson, L., Majumdar, A., Vestweber, D., Uv, A., and Betsholtz, C. (2012) The sphingosine-1-phosphate receptor S1PR1 restricts sprouting angiogenesis by regulating the interplay between VE-cadherin and VEGFR2. *Dev Cell* **23**, 587-599
64. Bentley, K., Franco, C. A., Philippides, A., Blanco, R., Dierkes, M., Gebala, V., Stanchi, F., Jones, M., Aspalter, I. M., Cagna, G., Westrom, S., Claesson-Welsh, L., Vestweber, D., and Gerhardt, H. (2014) The role of differential VE-cadherin dynamics in cell rearrangement during angiogenesis. *Nat Cell Biol* **16**, 309-321
65. Yamamoto, H., Ehling, M., Kato, K., Kanai, K., van Lessen, M., Frye, M., Zeuschner, D., Nakayama, M., Vestweber, D., and Adams, R. H. (2015) Integrin beta1 controls VE-cadherin localization and blood vessel stability. *Nat Commun* **6**, 6429
66. Calera, M. R., Venkatakrishnan, A., and Kazlauskas, A. (2004) VE-cadherin increases the half-life of VEGF receptor 2. *Exp Cell Res* **300**, 248-256
67. Abraham, S., Yeo, M., Montero-Balaguer, M., Paterson, H., Dejana, E., Marshall, C. J., and Mavria, G. (2009) VE-Cadherin-mediated cell-cell interaction suppresses sprouting via signaling to MLC2 phosphorylation. *Curr Biol* **19**, 668-674
68. Kanerva, K., Uronen, R. L., Blom, T., Li, S., Bittman, R., Lappalainen, P., Peränen, J., Raposo, G., and Ikonen, E. (2013) LDL cholesterol recycles to the plasma membrane via a Rab8a-Myosin5b-actin-dependent membrane transport route. *Dev Cell* **27**, 249-262

69. Zhao, K., Foster, J., and Ridgway, N. D. (2020) Oxysterol-binding protein-related protein 1 variants have opposing cholesterol transport activities from the endolysosomes. *Mol Biol Cell* **31**, 793-802

Table 1. Angiogenic signaling pathways affected in the transcriptome of ORP2 knock-down HUVECs (RNAseq), and in the peptide IDs of ORP2 interactome (MS) predicted by ConsensusPathDB pathway tool. Pathway databases included in the analysis: Wikipathways, KEGG, Reactome and PID (full lists of significant pathways in ORP2 KD RNAseq and ORP2-2xStrep mass spectrometric data are available upon request from the authors).

Signaling pathway	Affected genes/ tot. genes (RNAseq)	(%)	Identical gene IDs/ tot. genes (MS)	(%)	Adjust. p-value (RNAseq)	Adjust. p-value (MS)
VEGF-VEGFR2 signaling[37]	181/236	(76.7)	24/236	(10.2)	2.82^{-18}	1.65^{-08}
Cell migration	78/103	(75.7)	9/103	(8.7)	-	-
Cell proliferation	52/70	(74.3)	7/70	(10.0)	-	-
Cell survival	68/94	(72.3)	10/94	(10.6)	-	-
VEGFR endocytosis and recycling	23/30	(76.7)	9/30	(30.0)	-	-
Rho GTPase signaling	277/435	(63.7)	19/435	(4.4)	9.02^{-11}	2.05^{-02}
TGF-β signaling	101/132	(76.5)	10/132	(7.6)	1.09^{-10}	2.66^{-03}
EGF-EGFR signaling	117/162	(72.2)	9/162	(5.6)	1.94^{-09}	2.85^{-02}
Signaling by Hedgehog	84/96	(87.5)	-	-	3.23^{-08}	-
Signaling by RTKs	262/423	(61.9)	23/423	(5.4)	6.89^{-08}	8.97^{-04}
TNF-α signaling	71/93	(76.3)	-	-	7.58^{-08}	-
PDGFR-β signaling	92/127	(72.4)	14/127	(11.0)	8.07^{-08}	6.63^{-06}
FAK signaling	131/198	(66.2)	19/198	(9.6)	9.99^{-07}	2.58^{-09}
Notch signaling	61/79	(77.2)	-	-	1.36^{-07}	-
JAK-STAT signaling	75/106	(70.8)	-	-	5.42^{-06}	-
mTOR signaling	49/65	(75.8)	-	-	6.96^{-06}	-
Cdc42 signaling	53/71	(74.7)	-	-	1.09^{-05}	-
PI3K/Akt signaling	29/35	(82.9)	19/353	(4.3)	4.05^{-05}	2.76^{-03}
HIF-1-α signaling	48/66	(72.7)	5/66	(7.6)	8.75^{-05}	3.03^{-02}
EPH-Ephrin signaling	52/74	(70.3)	9/74	(12.2)	1.95^{-04}	1.40^{-04}
MAPK signaling	135/237	(56.7)	11/237	(4.6)	8.29^{-03}	4.97^{-02}

Table 2. Angiogenic cellular functions affected in the transcriptome of ORP2 knock-down HUVECs (RNAseq), and the peptide IDs of ORP2 interactome (MS) predicted by ConsensusPathDB gene ontology (GO) analysis tool (full lists of significant GO terms in ORP2 KD RNAseq and ORP2-2xStrep mass spectrometric data are available upon request from the authors).

Cellular function	GO term	Adj. p-value (RNAseq)	Adjust. p-value (MS)
Angiogenesis	GO:0001525	1.44^{-16}	1.06^{-03}
Cardiovascular system development	GO:0072358	8.06^{-21}	9.55^{-04}
Circulatory system development	GO:0072359	3.12^{-20}	2.07^{-03}
Vasculature development	GO:0001944	4.21^{-20}	7.87^{-04}
Blood vessel development	GO:0001568	4.53^{-19}	4.18^{-04}
Tube morphogenesis	GO:0035239	4.25^{-16}	7.89^{-03}
Blood vessel morphogenesis	GO:0048514	5.64^{-16}	3.50^{-03}
Tube development	GO:0035295	8.90^{-14}	5.76^{-04}
Regulation of vasculature development	GO:1901342	2.16^{-09}	-
Regulation of angiogenesis	GO:0045765	1.05^{-08}	3.06^{-02}
Sprouting angiogenesis	GO:0002040	3.54^{-08}	8.96^{-03}
Response to hypoxia	GO:0001666	1.47^{-06}	1.04^{-02}
Tube closure	GO:0060606	9.03^{-05}	-
Blood vessel remodeling	GO:0001974	4.66^{-04}	-
Vasculogenesis	GO:0001570	1.02^{-03}	4.13^{-03}
VEGF production	GO:0010573	7.94^{-03}	-

Table 3. Cholesterol homeostasis-related cellular functions affected in the transcriptome of ORP2 knock-down HUVECs (RNAseq), and the peptide IDs of ORP2 interactome (MS) predicted by ConsensusPathDB gene ontology (GO) analysis tool (full lists of significant GO terms in ORP2 KD RNAseq and ORP2-2xStrep mass spectrometric data are available upon request from the authors).

Cellular function	GO term	Adj. p-value (RNAseq)	Adj. p-value (MS)
Lipid metabolic process	GO:0006629	4.33^{-09}	6.39^{-06}
Sterol biosynthetic process	GO:0016126	1.45^{-07}	1.18^{-05}
Regulation of cholesterol metabolic process	GO:0090181	2.91^{-06}	1.31^{-04}
LDL particle clearance	GO:0034383	2.02^{-03}	3.73^{-06}
Cholesterol metabolic process	GO:0008203	3.18^{-05}	9.98^{-07}
Sterol metabolic process	GO:0016125	2.82^{-04}	4.23^{-06}
Steroid biosynthetic process	GO:0006694	5.69^{-03}	1.12^{-04}
Cholesterol storage	GO:0010878	7.31^{-03}	-
Phosphatidylinositol-mediated signaling	GO:0048015	7.71^{-03}	-
Steroid metabolic process	GO:0008202	-	6.96^{-06}
Plasma membrane organization	GO:0007009	6.87^{-03}	1.70^{-05}
Membrane raft organization	GO:0031579	-	5.17^{-05}
Membrane raft assembly	GO:0001765	1.90^{-03}	4.88^{-05}
Membrane raft localization	GO:0051665	-	5.81^{-03}

FIGURE CAPTIONS

Figure 1. ORP2 KD accumulates D4H-accessible cholesterol in late endosomes (LE) and ORP2 overexpression transfers it towards the plasma membrane (PM) in HUVECs. (A) Localization of the mCherry-D4H cholesterol probe in CTRL siRNA expressing HUVECs compared to ORP2 siRNA expressing HUVECs. Anti-LAMP1 was used as a LE marker and detected with Alexa488-conjugated secondary antibody. Nuclei were stained with Dapi. (B) Quantification of the mCherry-D4H probe LE and PM accumulation in ORP2 or CTRL siRNA expressing HUVECs. (C) Fluorescence microscopy images of the localization of the mCherry-D4H cholesterol probe, and (D) quantification of the LE and PM accumulation of the D4H probe in pEGFP-C1 control plasmid, ORP2(wt)-pEGFP-C1, ORP2(mHHK)-pEGFP-C1 or ORP2ΔELSK-pEGFP-C1 transfected HUVECs. The distribution of the D4H probe to LEs or PM is expressed as percentage of all analyzed D4H expressing cells. Approximately 100 cells with equal expression levels of the transfected constructs were analyzed for each transfection (n=3). The statistical significance (Student's t-test) is defined in comparison to control as ns, not significant, * $p<0.05$, ** $p<0.01$, *** $p<0.001$. Error bars represent ± SD.

Figure 2. Impacts of ORP2 knock-down (KD) on plasma membrane (PM) cholesterol and PI(4,5)P_2 content. (A) Relative PM cholesterol content in control (shC) and ORP2 KD (shO2) HUVECs measured from isolated PM preparations by Amplex Red assay. (B) Representative western blot of PM-association of growing concentrations (0 μM, 3 μM and 10 μM) of His_6-ALOD4 cholesterol probe in control cells, ORP2 KD cells, and cells depleted of PM cholesterol by 30-min by methyl-β-cyclodextrin (MβCD) treatment. (C) *In situ* quantification of PI(4,5)P_2 at the PM of control and ORP2 KD HUVECs. The images show spatially resolved PI(4,5)P_2 concentration in the cross-section of a representative cell at a timepoint 0. A pseudo-coloring scheme with red representing the highest and blue the lowest concentration is used to illustrate the spatial concentration heterogeneity. Similar spatially heterogenous distribution was observed at different time points. Scale bars represent 10 μm. (D) Relative PM PI(4,5)P_2 content of control and ORP2 KD cells measured from isolated PM preparations by competitive PI(4,5)P_2 ELISA. The statistical significance (Student's t-

test) is defined in comparison to control as ns, not significant, * $p<0.05$, ** $p<0.01$, *** $p<0.001$. Error bars represent ± SD.

Figure 3. Impacts of ORP2 manipulation on HUVEC protrusion and angiogenic network formation. (A) Representative images of protrusion formation in ORP2(wt)-pEGFP-C1 expressing HUVECs as compared to pEGFP-C1 control plasmid expressing HUVECs in basal cell culture conditions. (B) Quantification of HUVEC protrusion formation shown as percentage of transfected cells with prominent protrusions in ORP2(wt)- pEGFP-C1, ORP2(mHHK)-pEGFP-C1 and ORP2(ΔELSK)-pEGFP-C1 overexpressing cells in basal cell culture conditions. Empty plasmid (pEGFP-C1) was used as a control. For each transfection ≥ 100 cells were analyzed (n=3). (C) Representative images of angiogenic tubular network in lentivirally silenced control HUVECs (shCTRL) ORP2 knock-down (shORP2) HUVECs in the absence or presence of treatment with methyl-β-cyclodextrin-cholesterol complexes (+ chol). Images were taken 5 hours after cell seeding on matrix, with 4x magnification and analyzed with Angiogenesis Analyzer plugin of ImageJ (overlay of analysis shown in black) (D) Quantification of angiogenic tube formation parameters: number of tubular nodes, junctions, meshes, segments and branches, and total branching length in the absence (-) or presence (+) of 3-hour treatment with methyl-β-cyclodextrin-cholesterol complexes. The statistical significance (Student's t-test) is defined in comparison to control as ns, not significant, * $p<0.05$, ** $p<0.01$, *** $p<0.001$. Error bars represent ± SD.

Figure 4. ORP2 knock-down attenuates the activity of several angiogenic regulatory proteins and reduces the expression of PM lipid raft-associated proteins Caveolin-1 and VE-cadherin. (A) Western blot analysis of VEGFR2 phosphorylation in shCTRL (shC) and shORP2 (shO2) lentivirus-transduced HUVECs after 0-, 3- and 12-min treatment with VEGF-A_{165}. (B) Representative western blots and quantification of VEGFR2, Akt, eNOS3 and p70S6K phosphorylation upon 12-min VEGF-A_{165} stimulus in shORP2 and shCTRL expressing HUVECs (n ≥ 3). (C) Representative western blots of VEGFR2, Akt, eNOS3 and p70S6K phosphorylation upon 12-min VEGF-A_{165} stimulus in naïve (-) and cholesterol-depleted (+) HUVECs. tot = total protein, p = phosphorylated protein. Lanes showing the total protein on the western

filters are shown in Supplementary Fig. S2B,C. (D) The expression of Caveolin-1 and VE-cadherin quantified from shORP2 and shCTRL total cell lysate western blots ($n \geq 3$). (E) The expression of Flotillin-1 and Annexin A2 detected from shCTRL (shC) and shORP2 (shO2) total cell lysates by western blotting. The statistical significance (Student's t-test) is defined in comparison to shCTRL as * $p<0.05$, ** $p<0.01$, *** $p<0.001$. Error bars represent ± SD.

Figure 5. ORP2 knock-down impairs several angiogenic cell functions. (A) Representative proliferation graphs of ORP2 knock-down (shORP2) HUVECs compared to control (shCTRL) HUVECs. The cells were seeded as a sub-confluent monolayer on an xCELLigence® microelectrode biosensor and monitored in real-time for 20 h. (B) Viability of shORP2 HUVECs compared to shCTRL HUVECs determined by MTT assay performed on a confluent monolayer 12-h incubation with VEGF-A_{165}. Data is from four independent experiment each performed in five parallel wells. (C) Representative images of wound closure of ORP2 KD HUVECs compared to CTRL HUVECs plated on fibronectin-gelatin-coated 96-well plates, wounded with an IncuCyte® Wound Maker, and imaged before and after a 24-h incubation in IncuCyte ZOOM® system in basal growth media (D) Representative wound closure graphs of shORP2 and shCTRL HUVECs incubated for 20 hours and analyzed by IncuCyte ZOOM® automated quantification system (E). Representative curves of growth-factor stimulated trans-filter migration of shORP2 HUVECs compared to shCTRL HUVEs measured in real-time with xCELLigence® cell impedance-based migration application. (F) Representative images of shORP2 and shCTRL cell morphology imaged with Evos XL Cell Imaging System. (G) Representative images of the actin cytoskeleton organization and focal adhesion assembly in shORP2 HUVECs as compared to shCTRL HUVECs identified by phalloidin and p-paxillin immunofluorescence staining. The statistical significance (Student's t-test) is defined in comparison to shCTRL as * $p<0.05$, ** $p<0.01$, *** $p<0.001$. Error bars represent ± SD.

Figure 6. ORP2 knock-down decreases compartmentation of VEGFR2 into plasma membrane (PM) lipid rafts, reduces lipid raft-associated cholesterol and increases VEGFR2 cleavage at the PM of HUVECs. (A) Representative western blots of detergent-free cell fractionation of shCTRL and shORP2 HUVECs. The distributions

of VEGFR2, Flotillin-1 and β-tubulin are shown. Fraction 4 represents buoyant lipid raft membranes, fractions 5 & 6 heavier membranes, and fractions 8 & 9 the cytosol. (B) Quantification of the relative abundance of VEGFR2 in the lipid raft membrane fraction (Fr.4) of shCTRL and shORP2 HUVECs. (C) Quantification of the relative cholesterol content in the lipid raft membrane fraction (Fr.4) and in the heavier membrane fractions (Fr. 5 & 6) of shCTRL and shORP2 HUVECs. (D) ORP2 was knocked down in HUVECs by lentiviral transduction and the PM receptors were isolated by cell surface biotinylation and NeutrAvidin pull-down. Full-length VEGFR2 (230 kDa) and its cleaved form (130 kDa) were identified with anti-VEGFR2 antibody by western blotting. Tot. = total amount of VEGFR2 in cell lysates, PM = PM pool of VEGFR2 isolated by NeutrAvidin pull-down, int. = intracellular pool of VEGFR2 (remaining sample after NeutrAvidin pull-down). (E) Quantification of the cleaved 130 kDa residue of VEGFR2 at the PM of shORP2 and shCTRL HUVECs as percentages of the total PM pool of VEGFR2 (130 kDa + 230 kDa). (F) PM pool of full-length (230 kDa) and cleaved (130 kDa) VEGFR2 in control and ORP2 KD cells in the absence (-) or presence (+) of o/n treatment with 5 μM MMPi Marimastat. (G) PM pool of full-length (230 kDa) and cleaved (130 kDa) VEGFR2 in control (CTRL) and ORP2(wt) (oexO2) lentivirus transduced HUVECs. (H) Left; PM pool of full-length and cleaved form of VEGFR2 in cells depleted of PM cholesterol by 0-min, 30-min or 60-min methyl-β-cyclodextrin treatment (MβCD). Right; The PM pool of full-length (230 kDa) and cleaved (130 kDa) VEGFR2 in cells depleted of PM cholesterol by 30-min MβCD incubation in the absence (-) or presence (+) of o/n treatment with 5 μM MMPi Marimastat. The statistical significance (Student's t-test) is defined in comparison to shCTRL as * $p<0.05$, ** $p<0.01$, *** $p<0.001$. Error bars represent ± SD.

Figure 7. Loss of ORP2 results in dysregulation of retinal angiogenesis. Retinas from control (WT) and ORP2 knock out ($ORP2^{-/-}$) P7 littermate pups were analyzed by isolectin B4 immunostaining. (A) Confocal images of two different levels (1, 2) of retinas are shown as indicated. The superficial vascular plexus (1) is morphologically altered, and the extension of perpendicular endothelial sprouts (2) is significantly enhanced in $ORP2^{-/-}$ pup retinas. Bars, 200 μm. (B, C) The quantification of vessel length, endothelial cell (EC) area/field, branch points and perpendicular endothelial

sprouts in front and central areas of the control (WT) and ORP2 KO ($ORP2^{-/-}$) retinas from confocal microscopy images. The perpendicular sprouts were imaged form a focal plane underneath the vascular plexus. (C) Isolectin B4 immunofluorescence staining and tip cell quantification showing increased tip cell and filopodia extension at the angiogenic front of the $ORP2^{-/-}$ P7 pup retinas. Bars, 100 μm. (D) qPCR quantification of the Notch pathway mRNAs encoding cyclin D1 (CCND1), Delta-like protein 1 (DLL1), Jagged 1 (JAG1) and signal transducer and activator of transcription 1 (STAT1), mRNAs encoding cholesterol homeostatic components Farnesyl-Diphosphate Farnesyltransferase 1 (FDFT1) and Sterol Regulatory Element Binding Transcription Factor 2 (SREBF2) as well as mRNAs of cell-cell contact regulating VE-cadherin (CDH5) and a nod involved in Notch and VEGF signaling and in cholesterol biosynthesis, Mammalian Target Of Rapamycin (mTOR). The statistical significance (Student's t-test) is defined as ns, not significant, * $p<0.05$, ** $p<0.01$, *** $p<0.001$. Error bars represent ± SD.

Figure 1

Figure 1

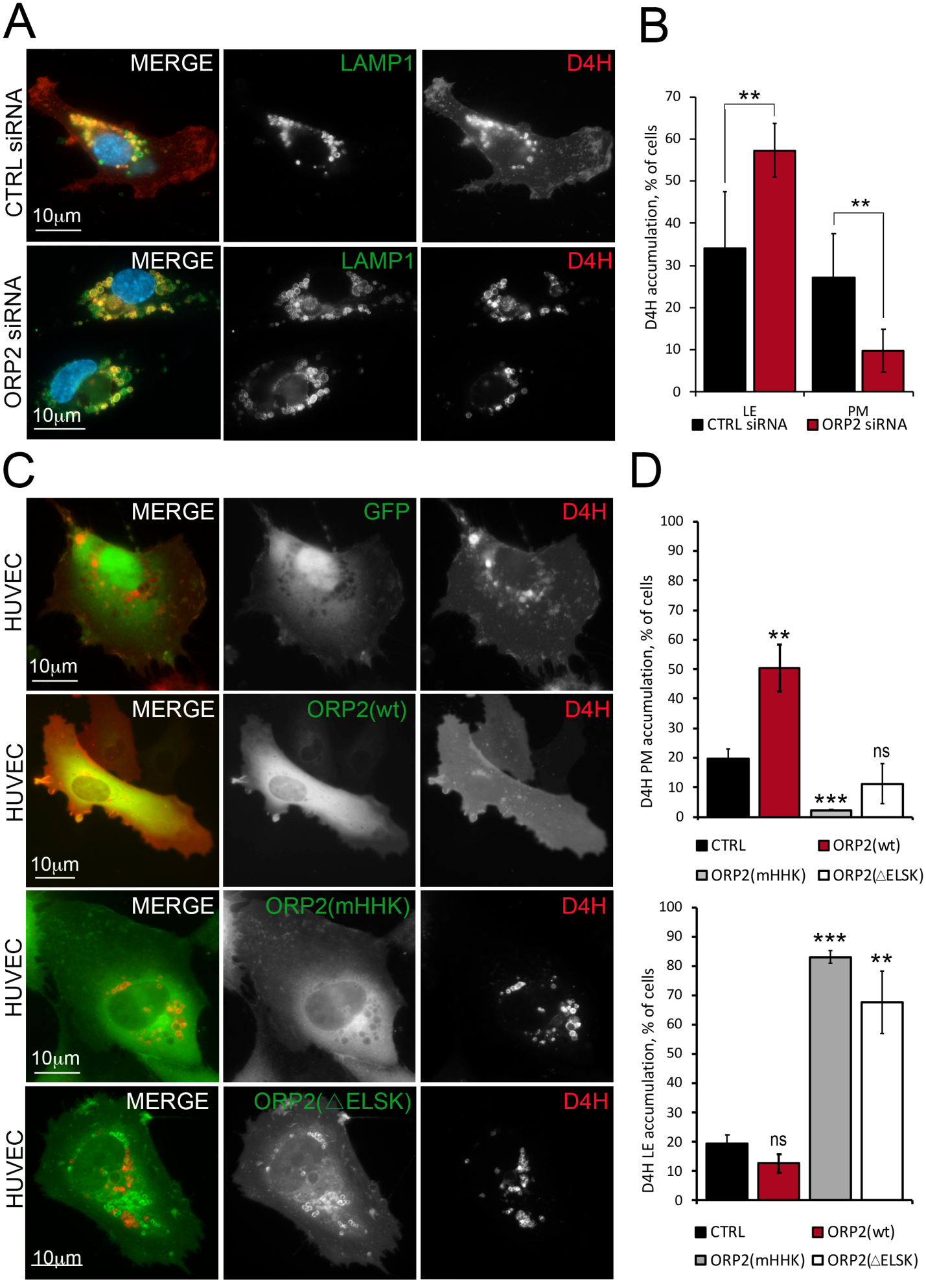

Figure 2

Figure 2

A

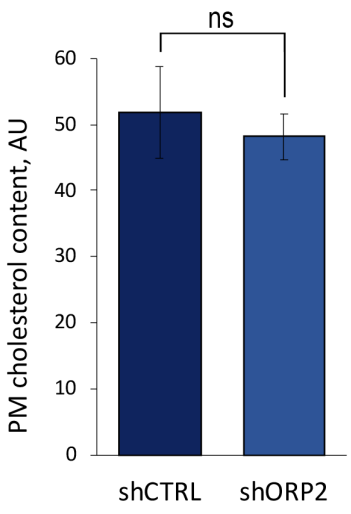

B

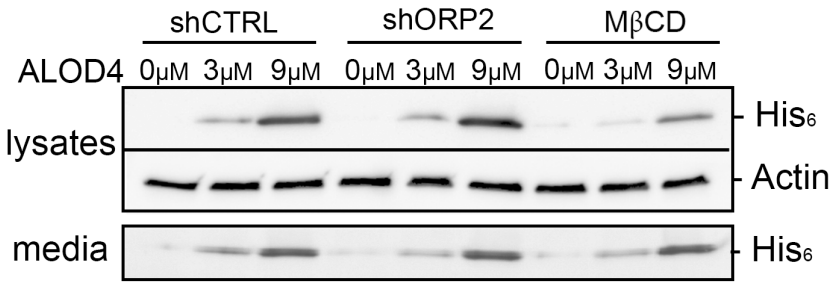

C

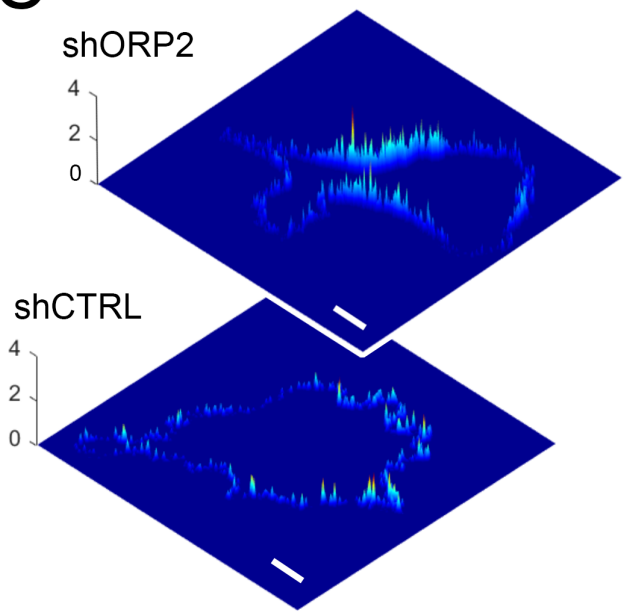

D

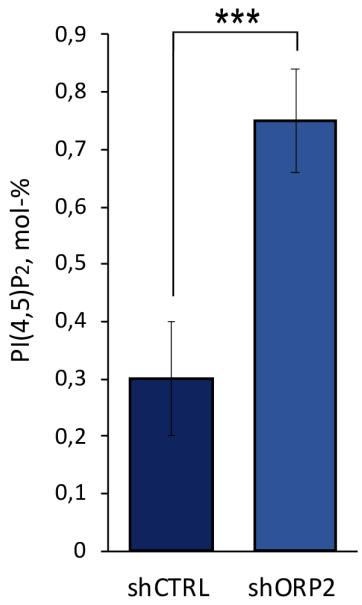

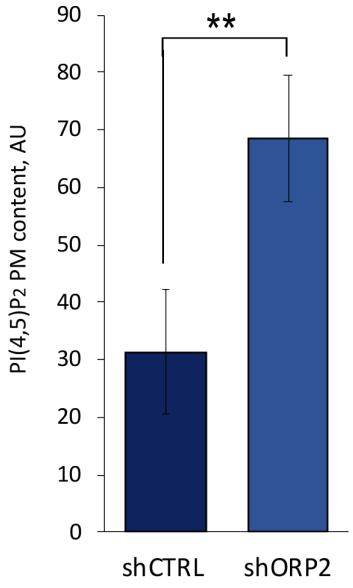

Figure 3

Figure 3

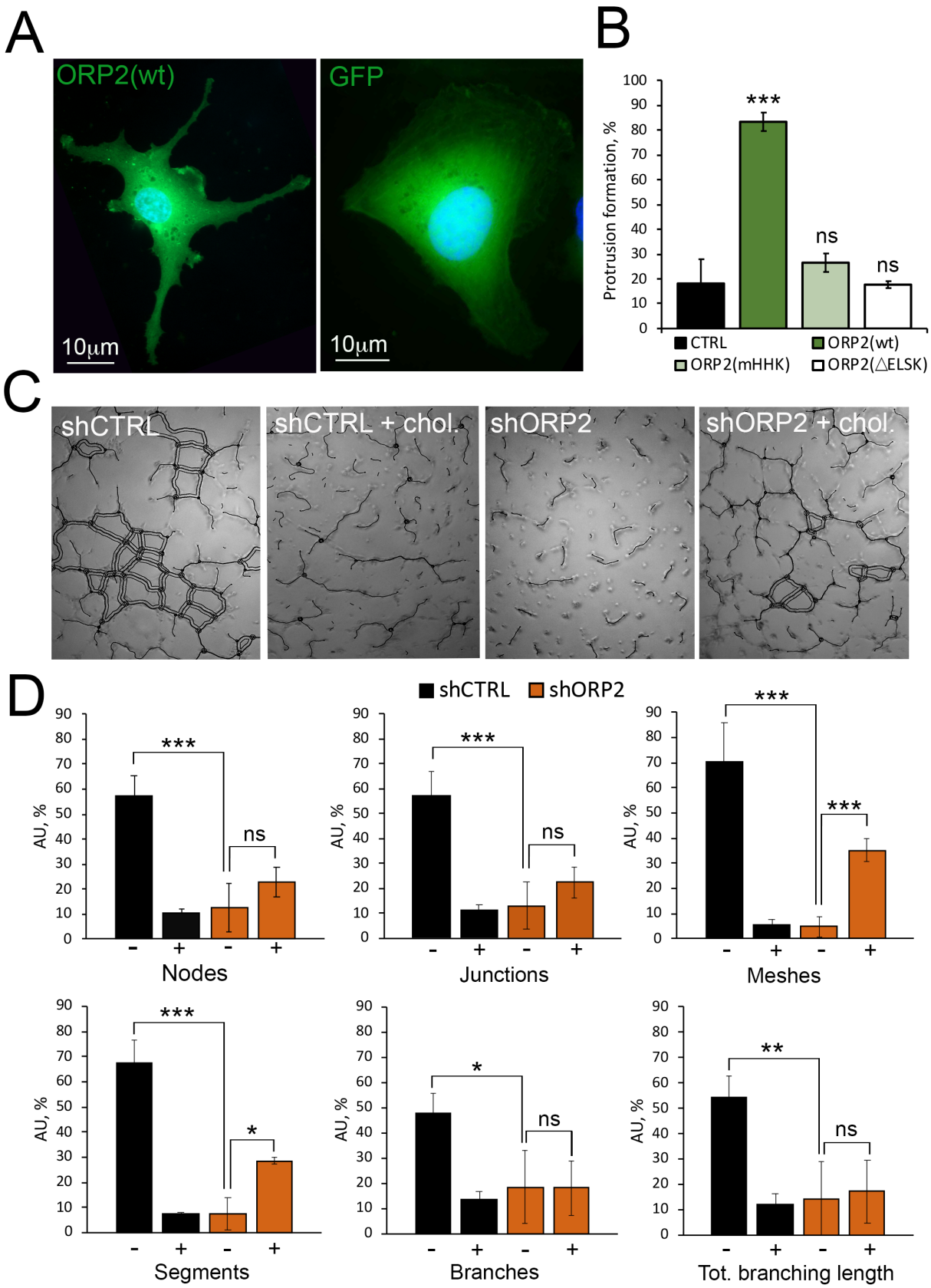

Figure 4

Figure 4

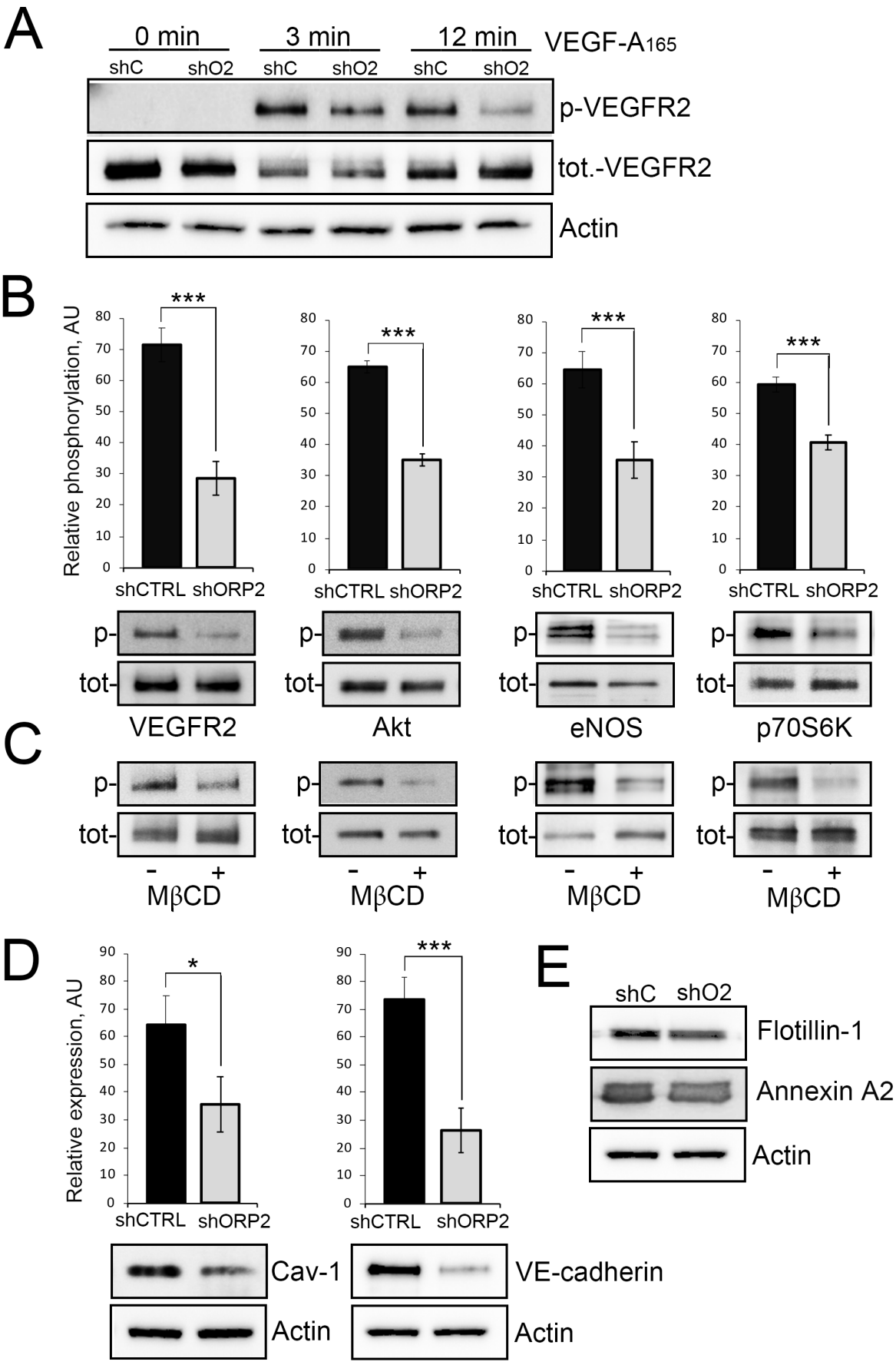

Figure 5

Figure 5

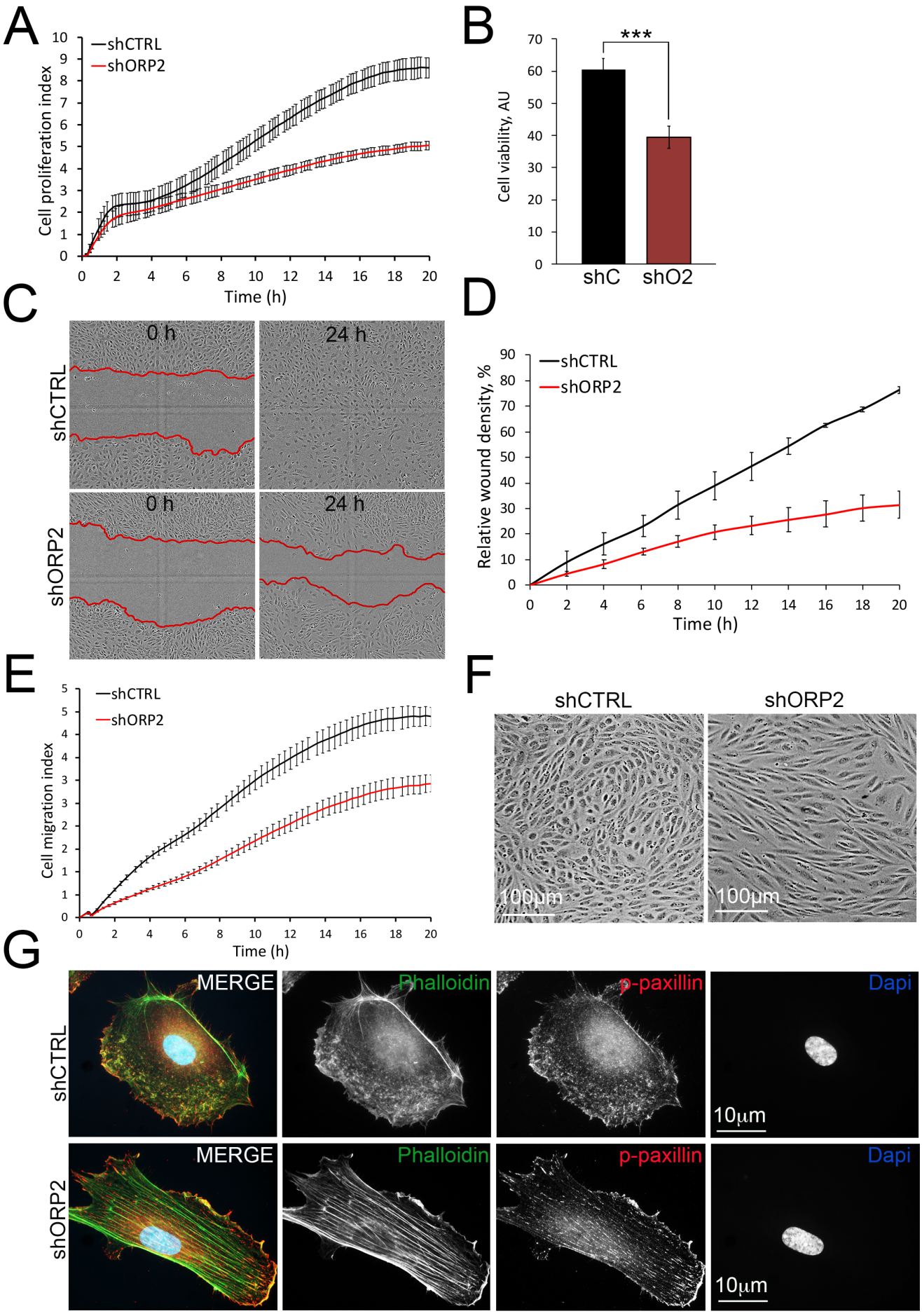

Figure 6

Figure 6

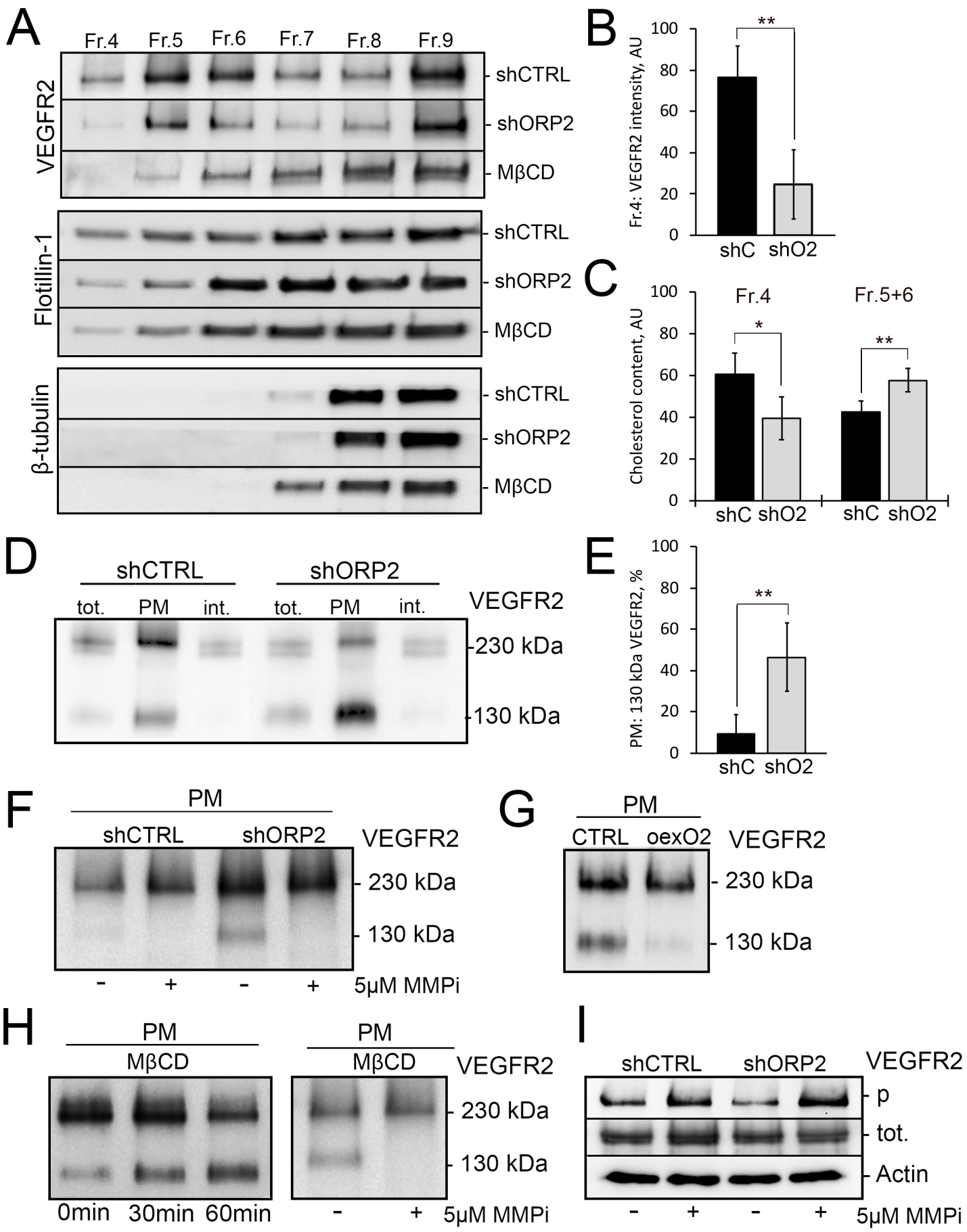

Figure 7

Figure 7

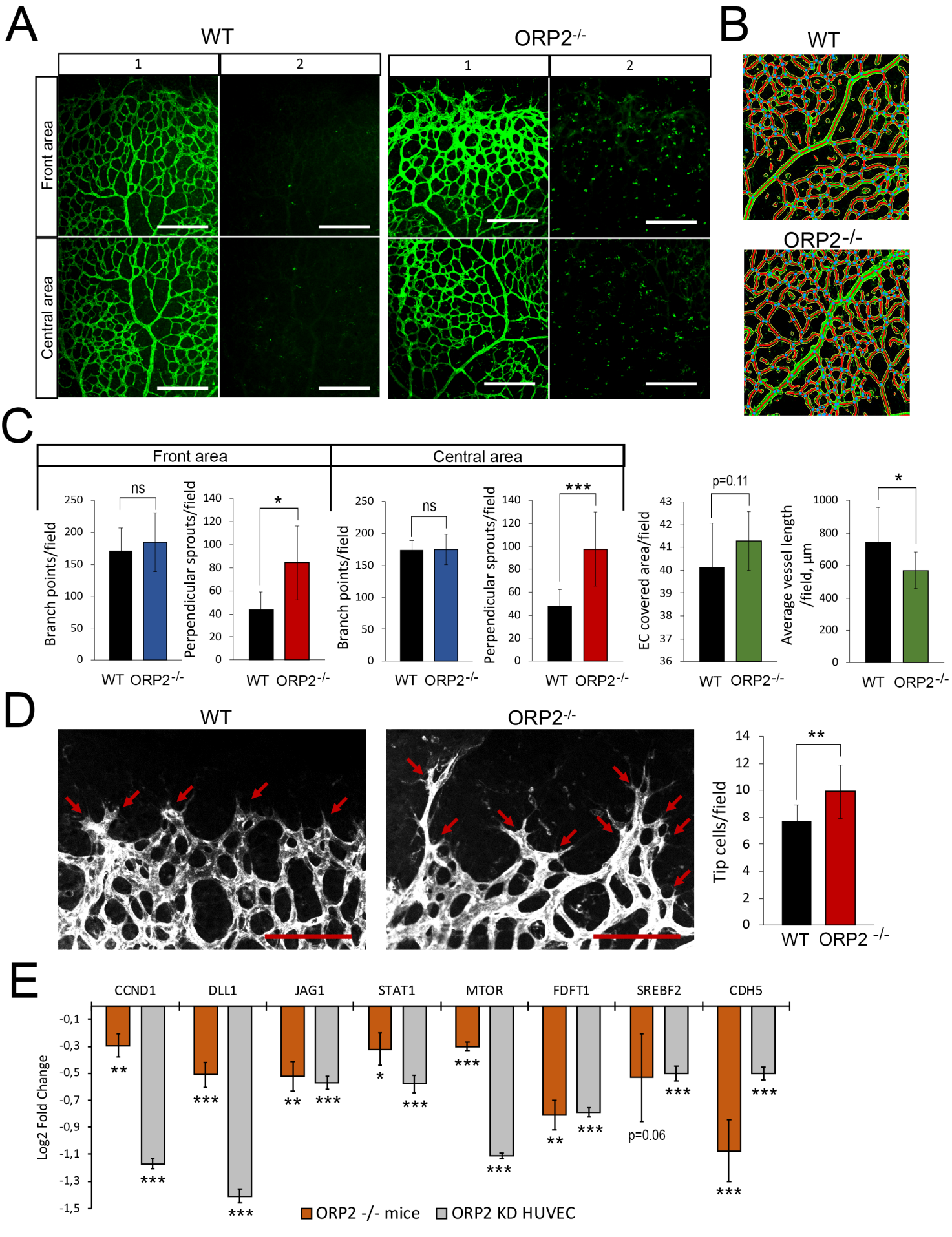

Supplementary Figure S1

A

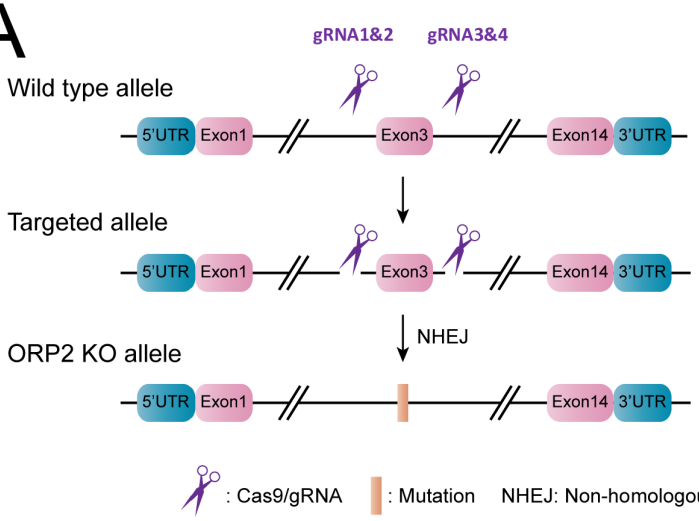

gRNA	Sequence(5'-3')
gRNA1	TCTGTTGCCTACTCGGTGAAAGG
gRNA2	TTGCCTACTCGGTGAAAGGATGG
gRNA3	CTGTGGATCATGTTATGTACAGG
gRNA4	GTACAGGCTGTGAACCATCCTGG

B

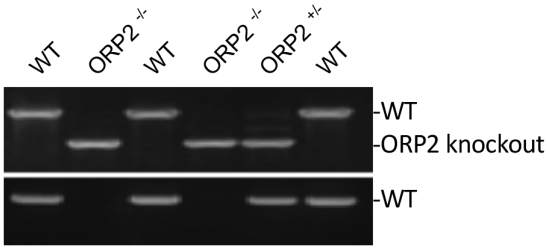

C

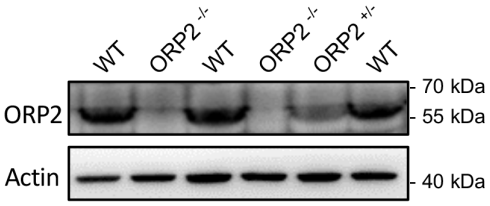

D

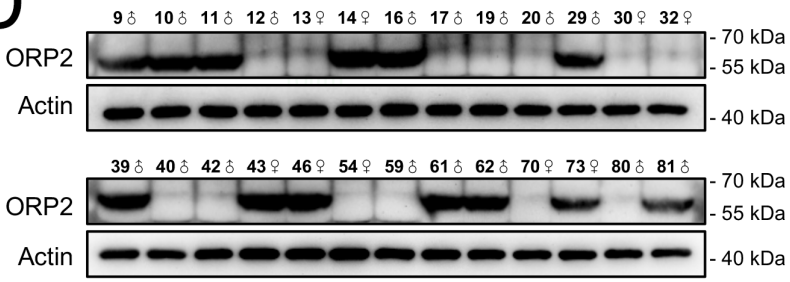

E

GENE/mRNA	Forward Primer	Reverse Primer
CCND1	GCGTACCCTGACACCAATCTC	ACTTGAAGTAAGATACGGAGGGC
DLL1	CCCATCCGATTCCCCTTCG	GGTTTTCTGTTGCGAGGTCATC
JAG1	TTCTCACTCAGGCATGATAAACC	CATCTCTGGGACGACAGAACT
STAT1	AGGATCAAGTCATGTGCATAGAGC	ACCATTGGCTTCACCTTCTCTGT
MTOR	GAAATTTGATCAGGTGTGCCAGTG	CTGGAGGTACTGGGTATCTGTGAA
FDFT1	ATGGAGTTCGTCAAGTGTCTAGG	CGTGCCGTATGTCCCCATC
SREBF2	GCAGCAACGGGACCATTCT	AGACTTGTGCATCTTGGCATCTG
CDH5	GAGAGACTGGATTTGGAATCAAATGCAC	CTCATAGGCAAGCACATTCCCTGTG

10μm

10μm

Supplementary Fig. S1 Generation of ORP2 knock-out (KO) mice. (A) ORP2 KO generation strategy (left) and gRNAs (right) used for ORP2 KO mice generation. ORP2 KO mice were generated by CRISPR/Cas9. Exon 3 for ORP2 was removed by targeting flanking intronic regions with four gRNAs. (B) Representative genotype analysis by PCR from ORP2 KO and WT mouse tail and (C) Western blot analysis of ORP2 KO and WT mouse brain tissue. (D) Western blot analysis of ORP2 KO mice and littermate WT pups used for the retinal analysis. (E) Primer sequences used for ORP2 KO and WT mice qPCR gene expression analysis.

Supplementary Figure S2

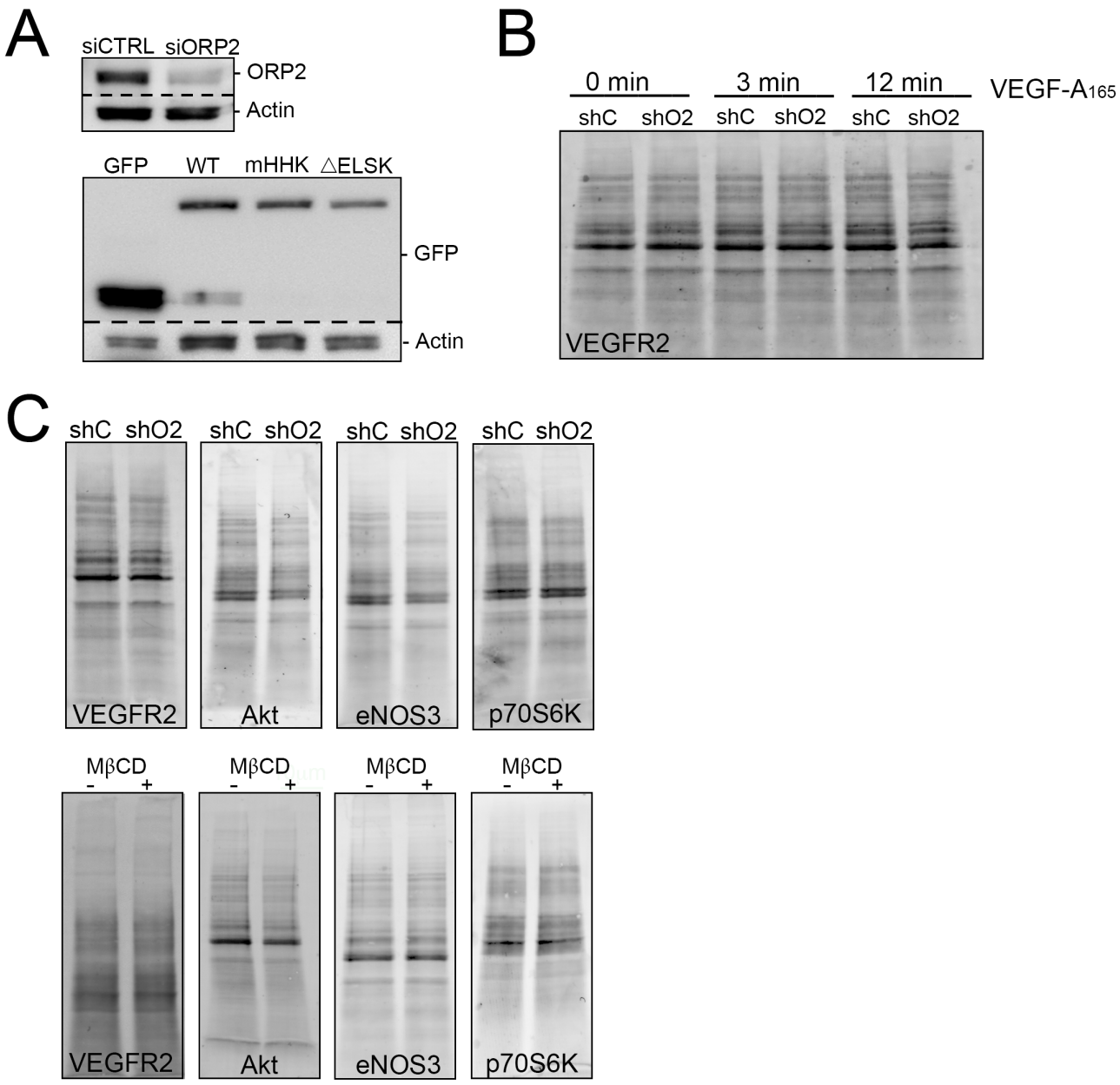

Supplementary Fig. S2 (A) Upper panel: Representative western blot of endogenous ORP2 expression in HUVECs transfected with either CTRL or ORP2 specific siRNA and detected with anti-ORP2 antibody. Lower panel: Representative western blot of pEGFP-C1, ORP2(wt)-pEGFP-C1, ORP2(mHHK)-pEGFP-C1 and ORP2(ΔELSK)-pEGFP-C1 overexpressing HUVECs detected with anti-GFP antibody. Actin is shown as a loading control and detected with β-actin antibody. (B) Total protein blot of shCTRL and shORP2 lentivirus-transduced HUVECs treated with VEGF-A_{165} for 0, 3 or 12 minutes (corresponds to western blot detected with anti-phospho-VEGFR2 shown in Fig.4A). (C) Total protein blot of shCTRL and shORP2 lentivirus-transduced HUVECs (upper panels) or naïve HUVECs depleted of plasma membrane cholesterol by methyl-β -cyclodextrin (lower panels), treated with VEGF-A_{165} for 12 minutes (correspond to western blots detected with anti-phospho-VEGFR2, -Akt, -eNOS or -p70S6K antibodies shown in Fig.4B).

Supplementary Figure S3

A

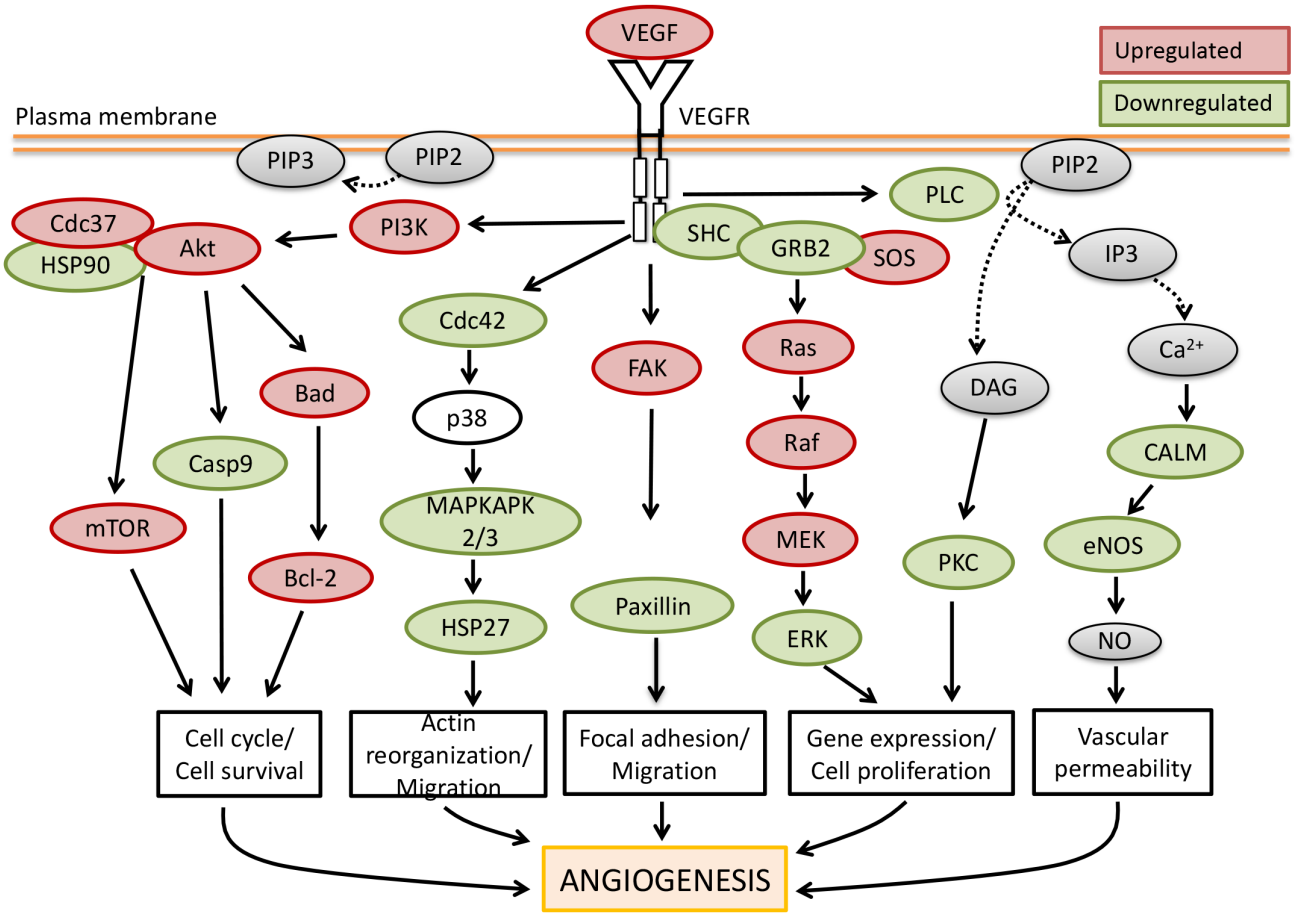

B

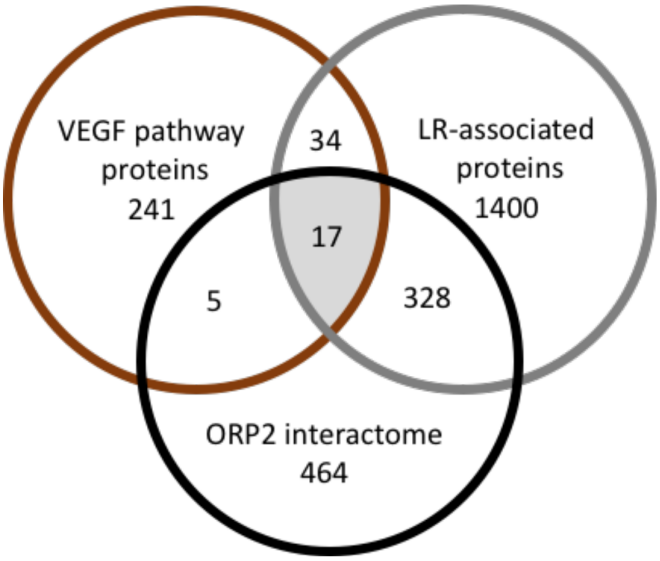

Gene ID	Description
CAV1	Caveolin-1
CDH5	Vascular endothelial cadherin
CLTC	Clathrin heavy chain 1
CTNNA1	Catenin alpha 1
CTNND1	Catenin delta 1
FLNB	Filamin-B
HSP90A	Heat shock protein 90 alpha
HSPA1A	Heat shock 70 kDa protein 1A
IQGAP1	IQ motif containing GTPase activating protein 1
ITGAV	Integrin alpha V
ITGB1	Integrin beta 1
MYH9	Myosin-9
RAB11A	Ras-related protein Rab-11A
RAP1B	Ras-related protein Rab-1B
RHOA	Ras homolog gene family. member A
RPS6	Ribosomal protein S6
VCL	Vinculin

Supplementary Fig. S3 (A) A schematic figure of the significantly affected genes in the VEGF-VEGFR2 signaling pathway in ORP2 KD HUVECs analyzed by RNAseq and ConsensusPathDB tool. Green = downregulated mRNAs; red = upregulated mRNAs. (B) VENN diagram of the VEGF pathway proteins (Wikipathways), lipid raft (LR) associated proteins (RaftProt database) and putative interaction partners of ORP2. The 17 proteins at the intercept of the three sections of the diagram are identified on the right.

Supplementary Table S1. List of the antibodies used

Antibody (anti-)	Source	Type	Manufacturer	Catalogue number
Akt	rabbit	polyclonal	Cell Signaling	9272
Annexin A2	rabbit	polyclonal	Abcam	ab178677
Caveolin-1 (clone 2297)	mouse	monoclonal	BD Transduction laboratories	610406
eNOS3	rabbit	polyclonal	Abcam	ab5589
ERK1/2	rabbit	polyclonal	Cell Signaling	9102
FAK (clone D-1)	mouse	monoclonal	Santa Cruz Biotechnology	sc-271126
Flotillin-1	rabbit	polyclonal	Cell Signaling	3253
GFP	rabbit	polyclonal	Molecular Probes	A-6455
His_6	mouse	monoclonal	ABclonal	AE003
LAMP1 (clone H4A3)	mouse	monoclonal	Santa Cruz Biotechnology	sc-20011
ORP2	rabbit	polyclonal	Novus Biologicals	92236
p70S6K	rabbit	polyclonal	Cell Signaling	9202
phospho-Akt(Ser473)	rabbit	polyclonal	Cell Signaling	9271
phospho-eNOS3(Ser1177)	rabbit	polyclonal	Cell Signaling	9571
phospho-ERK1/2(Thr202/Tyr204)	mouse	monoclonal	Cell Signaling	9106
phospho-FAK(Tyr397)	rabbit	monoclonal	Santa Cruz Biotechnology	8556T
phospho-p70S6K(Thr398)	rabbit	polyclonal	Cell Signaling	9205
phospho-Paxillin(Tyr118)	rabbit	polyclonal	Santa Cruz Biotechnology	sc-14036-R
phospho-VEGFR2(Tyr1175)	rabbit	monoclonal	Cell Signaling	2478
VE-cadherin (clone 123413)	mouse	monoclonal	R&D Systems	MAB9381-SP
VEGFR2 (clone 55B11)	rabbit	monoclonal	Cell Signaling	2479
β-actin	rabbit	polyclonal	Sigma-Aldrich	A2066
β-tubulin (clone AA2)	mouse	monoclonal	Merck	05-661

Supplementary Table S2. Cellular functions downstream of VEGF signaling associated with mRNAs of ORP2 knock-down HUVECs (RNAseq) and peptide IDs of ORP2 interactome (MS) predicted by ConsensusPath gene onthology (GO) analysis tool. (full lists of significant GO terms in ORP2 KD RNAseq and ORP2-2xStrep mass spectrometric data are available upon request from the authors)

Cellular function	GO term	Adj. p-value (RNAseq)	Adjust. p-value (MS)
Cell cycle	GO:0007049	1.97^{-39}	8.72^{-03}
Mitotic cell cycle	GO:0000278	8.08^{-32}	8.69^{-03}
Regulation of cell cycle	GO:0051726	1.27^{-26}	-
Cell division	GO:0051301	2.54^{-18}	3.83^{-03}
Regulation of cell proliferation	GO:0042127	1.61^{-11}	-
Cell growth	GO:0016049	1.97^{-09}	-
Cytoskeleton organization	GO:0007010	8.60^{-20}	1.48^{-08}
Actin cytoskeleton organization	GO:0030036	6.37^{-17}	3.56^{-07}
Actin filament organization	GO:0007015	1.95^{-12}	1.52^{-06}
Regulation of actin filament length	GO:0030832	7.91^{-06}	1.56^{-04}
Microtubule cytoskeleton organization	GO:0000226	1.24^{-07}	-
Actin polymerization or depolymerization	GO:0008154	4.19^{-06}	-
Cell death	GO:0008219	6.86^{-13}	3.81^{-09}
Apoptotic process	GO:0006915	3.94^{-17}	1.31^{-07}
Apoptotic signaling pathway	GO:0097190	2.37^{-16}	5.64^{-08}
Regulation of cell death	GO:0010941	1.85^{-13}	3.15^{-07}
Programmed cell death	GO:0012501	6.52^{-13}	1.60^{-08}
Necrotic cell death	GO:0070265	1.13^{-05}	2.49^{-03}
Cell motility	GO:0048870	1.24^{-06}	2.40^{-03}
Regulation of cell motility	GO:2000145	3.27^{-16}	5.02^{-04}
Regulation of locomotion	GO:0040012	5.18^{-16}	2.21^{-04}
Regulation of endothelial cell migration	GO:0010594	5.15^{-10}	-
Cell migration	GO:0016477	9.56^{-09}	1.01^{-03}
Wound healing	GO:0042060	3.19^{-04}	4.87^{-11}
Cell adhesion	GO:0007155	1.42^{-06}	1.64^{-07}
Cell-substrate adhesion	GO:0031589	2.78^{-10}	2.08^{-08}
Regulation of cell adhesion	GO:0030155	5.86^{-07}	1.11^{-04}
Substrate adhesion-dependent cell spreading	GO:0034446	1.77^{-06}	5.90^{-03}
Cell-matrix adhesion	GO:0007160	3.45^{-06}	3.73^{-06}
Cell-cell adhesion	GO:0098609	1.96^{-03}	6.76^{-04}

Supplementary Table S3. Significantly affected gene IDs of SREBP1 signaling pathway in ORP2 KD HUVECs. SREPB1 signaling pathway from WikiPathways database was used as a reference (described in Daemen, Kutmon & Evelo 2013: https://doi.org/10.1007/s12263-013-0342-x). Only pathways with p-value ≤0.05 are included.

Symbol	Description	log2FoldChange	p-adj.
MTOR	mechanistic target of rapamycin kinase [Source:HGNC Symbol;Acc:HGNC:3942]	-1.11	4.03E-162
FDFT1	farnesyl-diphosphate farnesyltransferase 1 [Source:HGNC Symbol;Acc:HGNC:3629]	-0.93	7.01E-131
MED15	mediator complex subunit 15 [Source:HGNC Symbol;Acc:HGNC:14248]	0.76	3.77E-101
SAR1B	secretion associated Ras related GTPase 1B [Source:HGNC Symbol;Acc:HGNC:10535]	0.88	1.08E-71
INSIG1	insulin induced gene 1 [Source:HGNC Symbol;Acc:HGNC:6083]	-0.94	2.04E-66
HMGCS1	3-hydroxy-3-methylglutaryl-CoA synthase 1 [Source:HGNC Symbol;Acc:HGNC:5007]	-0.79	6.42E-65
LSS	lanosterol synthase [Source:HGNC Symbol;Acc:HGNC:6708]	-0.7	1.36E-56
DBI	diazepam binding inhibitor. acyl-CoA binding protein [Source:HGNC Symbol;Acc:HGNC:2690]	-0.62	7.62E-47
SEC24C	SEC24 homolog C. COPII coat complex component [Source:HGNC Symbol;Acc:HGNC:10705]	0.42	1.10E-45
LDLR	low density lipoprotein receptor [Source:HGNC Symbol;Acc:HGNC:6547]	0.68	2.88E-43
SREBF2	sterol regulatory element binding transcription factor 2 [Source:HGNC Symbol;Acc:HGNC:11290]	-0.5	2.84E-39
FASN	fatty acid synthase [Source:HGNC Symbol;Acc:HGNC:3594]	-0.51	1.87E-36
IDI1	isopentenyl-diphosphate delta isomerase 1 [Source:HGNC Symbol;Acc:HGNC:5387]	-0.62	1.11E-34
SQLE	squalene epoxidase [Source:HGNC Symbol;Acc:HGNC:11279]	-0.56	4.89E-32
MVD	mevalonate diphosphate decarboxylase [Source:HGNC Symbol;Acc:HGNC:7529]	-0.67	2.74E-30
PRKAB2	protein kinase AMP-activated non-catalytic subunit beta 2 [Source:HGNC Symbol;Acc:HGNC:9379]	0.51	2.84E-28
SCD	stearoyl-CoA desaturase [Source:HGNC Symbol;Acc:HGNC:10571]	-0.54	2.19E-25
HMGCR	3-hydroxy-3-methylglutaryl-CoA reductase [Source:HGNC Symbol;Acc:HGNC:5006]	-0.38	5.64E-23
PRKAG1	protein kinase AMP-activated non-catalytic subunit gamma 1 [Source:HGNC Symbol;Acc:HGNC:9385]	-0.51	2.32E-21
SEC31A	SEC31 homolog A. COPII coat complex component [Source:HGNC Symbol;Acc:HGNC:17052]	0.31	2.77E-21
SEC13	SEC13 homolog. nuclear pore and COPII coat complex component [Source:HGNC Symbol;Acc:HGNC:10697]	0.28	1.68E-19
FDPS	farnesyl diphosphate synthase [Source:HGNC Symbol;Acc:HGNC:3631]	-0.25	2.04E-17
SCARB1	scavenger receptor class B member 1 [Source:HGNC Symbol;Acc:HGNC:1664]	-0.32	1.47E-16
NR1H2	nuclear receptor subfamily 1 group H member 2 [Source:HGNC Symbol;Acc:HGNC:7965]	0.27	1.51E-13
SEC23B	Sec23 homolog B. coat complex II component [Source:HGNC Symbol;Acc:HGNC:10702]	0.32	6.14E-13
ACSS1	acyl-CoA synthetase short chain family member 1 [Source:HGNC Symbol;Acc:HGNC:16091]	-0.63	1.44E-12
PIK3CA	phosphatidylinositol-4.5-bisphosphate 3-kinase catalytic subunit alpha [Source:HGNC Symbol;Acc:HGNC:8975]	0.32	5.12E-12

PRKAA1	protein kinase AMP-activated catalytic subunit alpha 1 [Source:HGNC Symbol;Acc:HGNC:9376]	-0.28	1.34E-11
ACLY	ATP citrate lyase [Source:HGNC Symbol;Acc:HGNC:115]	-0.23	2.13E-11
ACACA	acetyl-CoA carboxylase alpha [Source:HGNC Symbol;Acc:HGNC:84]	-0.3	2.63E-11
PRKACA	protein kinase cAMP-activated catalytic subunit alpha [Source:HGNC Symbol;Acc:HGNC:9380]	-0.26	1.06E-10
ATF6	activating transcription factor 6 [Source:HGNC Symbol;Acc:HGNC:791]	0.24	1.24E-10
SEC24D	SEC24 homolog D. COPII coat complex component [Source:HGNC Symbol;Acc:HGNC:10706]	0.24	1.86E-10
INSIG2	insulin induced gene 2 [Source:HGNC Symbol;Acc:HGNC:20452]	-0.32	2.44E-08
NFYA	nuclear transcription factor Y subunit alpha [Source:HGNC Symbol;Acc:HGNC:7804]	-0.25	5.74E-08
MBTPS2	membrane bound transcription factor peptidase. site 2 [Source:HGNC Symbol;Acc:HGNC:15455]	0.3	7.54E-08
MBTPS1	membrane bound transcription factor peptidase. site 1 [Source:HGNC Symbol;Acc:HGNC:15456]	0.19	1.05E-07
PPARGC1B	PPARG coactivator 1 beta [Source:HGNC Symbol;Acc:HGNC:30022]	0.5	5.88E-07
PRKAB1	protein kinase AMP-activated non-catalytic subunit beta 1 [Source:HGNC Symbol;Acc:HGNC:9378]	0.27	2.45E-06
LPIN1	lipin 1 [Source:HGNC Symbol;Acc:HGNC:13345]	-0.19	5.76E-06
SP1	Sp1 transcription factor [Source:HGNC Symbol;Acc:HGNC:11205]	-0.21	3.93E-05
KPNB1	karyopherin subunit beta 1 [Source:HGNC Symbol;Acc:HGNC:6400]	-0.16	5.08E-05
SAR1A	secretion associated Ras related GTPase 1A [Source:HGNC Symbol;Acc:HGNC:10534]	-0.15	9.02E-05
CYP51A1	cytochrome P450 family 51 subfamily A member 1 [Source:HGNC Symbol;Acc:HGNC:2649]	-0.38	6.24E-04
SEC24A	SEC24 homolog A. COPII coat complex component [Source:HGNC Symbol;Acc:HGNC:10703]	-0.15	8.66E-04
AMFR	autocrine motility factor receptor [Source:HGNC Symbol;Acc:HGNC:463]	0.12	2.05E-03
AKT1S1	AKT1 substrate 1 [Source:HGNC Symbol;Acc:HGNC:28426]	0.1	3.27E-03
PRKAA2	protein kinase AMP-activated catalytic subunit alpha 2 [Source:HGNC Symbol;Acc:HGNC:9377]	0.32	9.04E-03
RNF139	ring finger protein 139 [Source:HGNC Symbol;Acc:HGNC:17023]	0.15	1.06E-02
CDK8	cyclin dependent kinase 8 [Source:HGNC Symbol;Acc:HGNC:1779]	-0.16	1.16E-02
YY1	YY1 transcription factor [Source:HGNC Symbol;Acc:HGNC:12856]	-0.1	1.85E-02
GSK3A	glycogen synthase kinase 3 alpha [Source:HGNC Symbol;Acc:HGNC:4616]	0.11	2.46E-02
SIRT1	sirtuin 1 [Source:HGNC Symbol;Acc:HGNC:14929]	0.15	2.92E-02
SREBF1	sterol regulatory element binding transcription factor 1 [Source:HGNC Symbol;Acc:HGNC:11289]	0.09	3.52E-02